Tracking Barrier Island Response to Early Holocene Sea-level Rise: High Resolution Study of Estuarine Sediments in the Trinity River Paleovalley

Burstein, J.T.[1,†,*], Goff, J.A.[1], Gulick, S.P.S.[1,2], Lowery, C.[1], Standring, P.[1,2], Swartz, J.[1,#]

[1] University of Texas Institute for Geophysics, Jackson School of Geosciences, University of Texas at Austin, Austin, TX, USA

[2] Department of Geological Sciences, Jackson School of Geosciences, University of Texas at Austin, Austin, TX, USA

[#] Now at Water Institute of the Gulf, Baton Rouge, Louisiana

[†] Now at T. Baker Smith, Aransas Pass, Texas

[*] Corresponding Author: Jacob T. Burstein; email: jtburstein@utexas.edu

Abstract

Understanding how barrier islands respond to factors such as variations in sediment supply, relative sea-level rise, and accommodation is valuable for preparing coastal communities for future impacts of climate change. Increasingly, the underlying antecedent topography has been observed to have a significant control on the evolution of the barrier island system by providing increased elevation, decreased accommodation, and sediment supply for the barrier to rework and anchor upon. However, less attention has been focused on how back barrier sediments respond to this decreased accommodation, and how this may affect barrier island evolution. Additionally, the control in which the geometry of the underlying valley itself has on the initiation of barrier islands is poorly understood. Here we examine the stratigraphic

framework of the Trinity River incised valley, offshore Galveston, Texas in order to investigate the role of antecedent topography in the evolution of an ancient barrier island system. We present high-resolution imaging of the Trinity incised valley fill using over 1200 km² of 3D seismic, <700 km of 2D envelope and full waveform chirp data, along with 2 piston cores, 4 gravity cores, 1 platform boring, with associated grain size, foraminiferal, and radiocarbon data. We find that the geometry and elevation of the underlying antecedent topography plays a central role in the evolution of the barrier island system, promoting both initiation and stabilization. This study provides a methodology to investigate the evolution of a relict barrier island system where little to none of the barrier is preserved. With this methodology, we revise the established Holocene paleoshoreline model for the Trinity incised valley.

1. Introduction

Estuaries are uniquely dynamic depositional systems controlled by the interplay of river, wave, and tidal forces. They develop within incised valleys, which are formed through fluvial incision during periods of lower relative sea-level (Anderson et al., 2004; Nordfjord et al., 2006). Incised valleys act as topographic hollows, providing accommodation for subsequent lowstand and transgressive deposits (Vail 1977; Van Wagoner et al., 1988, 1990; Allen and Posamentier, 1993; Nordfjord et al., 2006). This accommodation provides protection from transgressive erosion, which cannibalizes older underlying sediment (Swift and Thorn, 1991; Cattaneo and Steel, 2003). Acting as sediment sinks for terrestrial, estuarine, and marine deposits, incised valleys provide a natural laboratory to investigate the rich depositional and erosional history of past sea-level cycles (Belknap and Kraft, 1981, 1985; Dalrymple et al., 1992; Allen and Posamentier, 1993, Zaitlin et al., 1994; Thomas, 1991; Thomas and Anderson, 1994; Cattaneo

and Steel, 2003; Anderson et al., 1996, 2004, 2008, 2014, 2016; Rodriguez et al., 2004, 2005;

Reijenstein et al., 2011).

Preserved estuarine sediments within incised valley fills enable comprehensive studies

investigating estuarine response to relative sea-level rise (Thomas and Anderson, 1994; Storms

et al., 2008; Simms et al., 2008; Rodriguez et al., 2004, 2005; Anderson et al., 2004, 2014, 2016;

Reijenstein et al., 2011; Ronchi et al., 2018, 2019; Shawler et al., 2020). In particular, the

Holocene estuarine record within the Gulf of Mexico incised valley fills have been extensively

studied due to excellent preservation and well-constrained rates of sea-level rise during this time

period (Milliken et al., 2008; Anderson et al., 2016). These studies have led to the commonly-

applied stratigraphic model of estuarine and barrier island response to episodic changes in

relative sea-level rise (Thomas and Anderson, 1994; Anderson et al., 2008; Anderson et al.,

2010), changes in climate, which regulates sediment supply (Anderson et al., 2008), and flooding

of antecedent fluvial topography (Rodriguez et al., 2004, 2005; Anderson et al., 2008) in the

form of flooding surfaces. In response to increased relative sea-level rise, decreased sediment

supply, or increased surface area of fluvial terraces, estuarine systems will experience rapid

landward back-stepping, wherein fluvial and bayhead delta sequences are overlain by bay, tidal,

barrier, and marine deposits. This results in an incised valley fill characterized by discontinuous,

landward-stepping, deepening-upward successions (Thomas and Anderson, 1994; Anderson et

al., 2016).

Antecedent topography is another factor that is increasingly understood to play a pivotal

role in controlling the evolution of estuarine and barrier island systems in a multitude of ways.

Previous authors found that flooding of antecedent fluvial terraces within the incised valley

results in increased surface area for rapid bay expansion (Rodriguez at al., 2005; Anderson et al.,

2008; Simms et al., 2008), while also serving as local sand sources to supply the transgressing barrier (Rodriguez et al., 2004). Through a comprehensive field and morphodynamic modelling study, Shawler et al. (2020) found that antecedent topographic highs play a central role in how barrier islands respond to sea-level rise. They found that steep antecedent slopes and decreased back-barrier accommodation provides both increased elevation and erodible sediment supply to essentially anchor the island despite high rates of sea-level rise, and thus promotes barrier resilience. Conversely, increased back-barrier accommodation may lead to rapid landward migration.

To investigate the role of antecedent topography in the evolution of an ancient barrier island system, we focus on the Trinity incised valley offshore modern Galveston Bay in the central Gulf of Mexico (Figure 1; Anderson et al., 2016). The regional estuarine stratigraphic framework has been previously studied, identifying fluvial and deltaic units overlain by estuarine units including lower bay and tidal-inlet sands (Thomas and Anderson, 1994; Anderson et al., 2004; Rodriguez at al., 2004, 2005; Swartz, 2019). Rates of RSLR in the northern Gulf of Mexico over the last 10 kyr are well-constrained, displaying a decrease from 5 mm yr^{-1} to 3 mm yr^{-1} (Milliken et al., 2008). However, previous authors have focused on identifying the adjustment and evolution of the fluvial-deltaic system during RSLR (Swartz, 2019), or have lacked the geophysical resolution to accurately identify fine-scale stratigraphic architecture necessary to capture the complex nature of the estuarine section (Thomas and Anderson, 1994; Anderson et al., 2004; Rodriguez at al., 2004, 2005).

In this study, we utilize a dense (~250 m line spacing) grid of high-resolution chirp data, in combination with micropaleontological, sedimentological, and radiocarbon dating methods to investigate the role of the antecedent geology on the initiation and evolution of a paleo-barrier

island system. This study provides a methodology to study the evolution of a paleo-barrier

system where little of the barrier itself is preserved in the stratigraphy. Using this methodology,

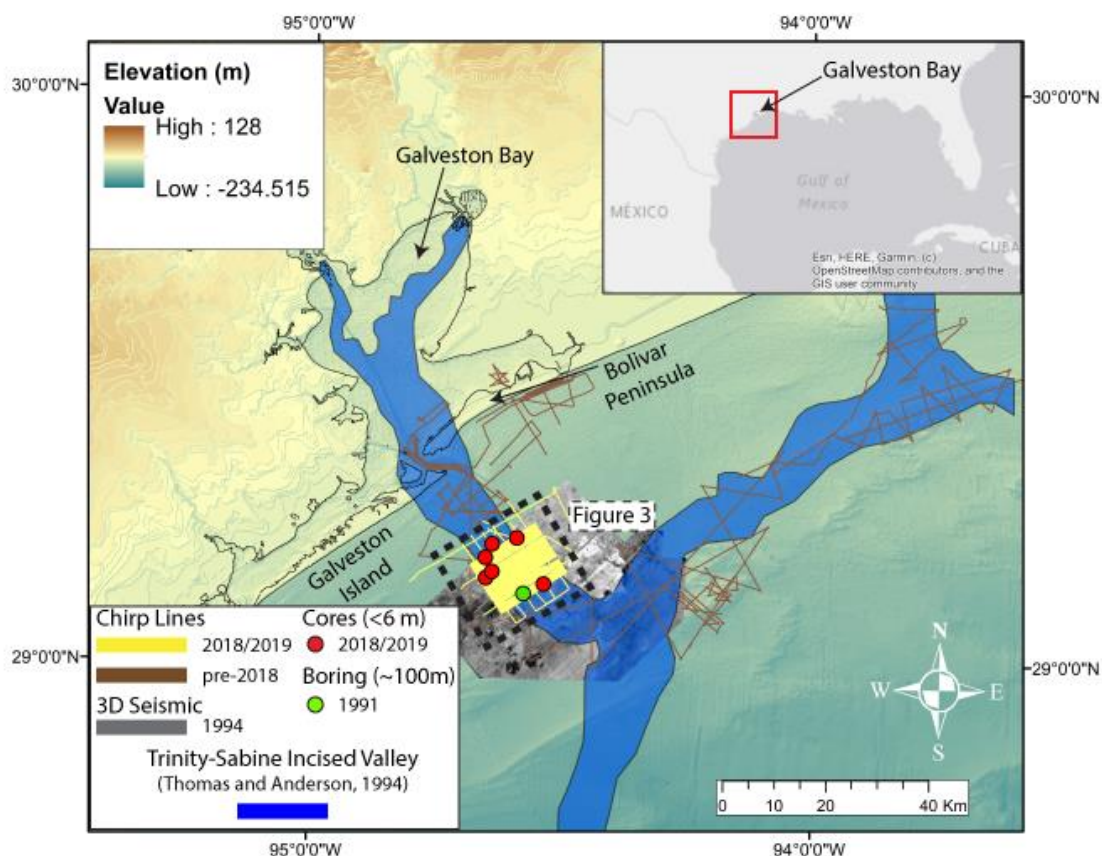we revise the established Holocene paleoshoreline model for the Trinity incised valley.

Figure 1. Map of the east Texas continental and inner shelf. Blue polygon represents the extent of the Trinity-Sabine

incised valley (modified from Thomas and Anderson, 1994). Brown tracklines represent available geophysical data

for the area. Yellow lines represent chirp geophysical data used in this study. Grey coherency extraction represent

spatial extent of publicly available, former industry collected 3D seismic data used in Swartz, 2019 and this study.

Red circles represent gravity and piston cores used in Standring et al., 2019 and this study. Green circle represents

Boring 4 from Thomas, 1991.

2. Study Area

The northern Gulf of Mexico experiences highly variable regional basin subsidence, exhibiting relatively low rates in coastal regions (0.03 mm/yr), yet high rates along the shelf edge (> 1.0 mm/yr) (Anderson et al., 2016). The central Texas region is currently classified as a dry subhumid region (Thornthwaite, 1948). However, multiple studies focused on the post-glacial climatic history of central Texas observe marked changes from cool and wet ~18 – 7.5 ka, to warm and dry ~7.5 to 3.5 ka, and finally variable, millennial scale shifts between cool-wet and warm-dry conditions since 3.5 ka (Humphrey and Ferring, 1994; Nordt et al., 1994, 2002; Toomey et al., 1993). The oceanographic circulation along the inner shelf is dominated by a strong westward current called the Louisiana Coastal Current (Cochane and Kelly, 1986; Oey 1995; Jarosz and Murray, 2005).

The Trinity incised valley formed during Marine Isotope Stages (MIS) 5-3, approximately 119 to 22 ka. During this time, the region experienced ~120 m in episodic sea-level fall, prompting a stepped downcutting of the fluvial system into the continental shelf. This resulted in an incised valley with a terraced morphology extending from the modern Galveston Bay to the shelf margin (Fig. 1; Thomas and Anderson, 1994; Anderson et al., 2016). The incised valley reached its most basinward location during MIS 2 approximately 22 to 17 ka, depositing a large shelf edge delta and basin floor fan complex (Pirmez et al., 2012; Anderson et al., 2016). Thomas and Anderson (1994) measured the valley surface to have 30-40 m of total relief; however, upper portions of the valley have since been infilled or removed by the transgressive ravinement during subsequent sea-level rise, and only lower portions of the valley exist offshore overlain by the seafloor.

Following the MIS2 lowstand, rapid sea-level rise (~4.2 mm/yr) between ~17 – 10 ka prompted a shift from progradation to aggradation, retrogradation, and valley filling for much of

the fluvial systems across the Gulf of Mexico (Milliken et al., 2008; Anderson et al., 2016). By 10 ka, the rate of sea level rise slowed progressively from 4.2 mm/yr to 1.4 mm/yr, leading to slower rates of transgression, better preservation of thick transgressive deposits, and, as a result, a more complete sedimentological record (Milliken et al., 2008; Anderson et al., 2014; 2016). After 10 ka, the Trinity valley was infilled by a series of discontinuous, landward stepping depositional packages consisting of fluvial, deltaic, bay and tidal packages (Thomas and Anderson, 1994; Rodriguez et al., 2004; Anderson et al., 2016).

Previous authors have interpreted large shelf sand bodies on the inner shelf as remnants of coastal barriers formed during sea-level stillstands, and subsequently overstepped and reworked during transgression (Rodriguez et al., 1999; 2004; Anderson et al., 2016). Rodriguez et al. (2004) identified estuarine muds overlain by shoreface and/or tidally influenced sands within cores beneath Heald Bank and Sabine Bank (Fig. 2). Ages acquired from the estuarine units at both locations suggest that estuaries existed at Heald Bank and Sabine Bank from 8.4 to 7.7 ka and 7.4 to 4.7 ka, respectively. Dates taken from estuarine packages in West and East Bay (Fig. 2) suggest that a lagoon existed in those areas since at least 7.5 and 7.7 ka, respectively. Thus, the shoreface and/or tidally influenced unit below Heald Bank was interpreted as the 7.7 ka barrier island location, fronting a 50-km long estuary extending from Heald Bank to West and East Bays (Rodriguez et al., 2004). These authors suggested that the western portion of the barrier shoreline rapidly retreated during RSLR until Galveston Island began prograding approximately 5.3 ka.

Conversely, according to Rodriguez et al. (2004), the eastern portion of the barrier shoreline remained relatively stable, reaching Sabine Bank around 5.3 ka, leading to an irregular, perpendicular shoreline extending from Sabine Bank to East Bay (Fig. 2). The shoreline

gradually retreated to the southwestern Louisiana chenier plain by 2.8 ka, and again to Bolivar

Peninsula by 1.5 ka as it began to form by spit creation, washover, and ephemeral flood-tidal

delta deposition (Fig. 2; Gould and McFarlan 1959). The stabilization, and subsequent rapid

retreat of the paleoshoreline has been attributed to the presence of fluvial deposits directly

beneath Heald and Sabine Banks within the Trinity-Sabine incised valley (Rodriguez et al.,

2004). As the shoreline retreated, the fluvial deposits provided both an anchor point and a local

sediment supply to remain relatively stable; however, once these sources were depleted and/or a

sediment supply-to-sea-level threshold was surpassed, rapid shoreline retreat ensued.

Alternatively, Thomas and Anderson, 1994 earlier proposed that these sand banks do not have

origins as submerged, overstepped barriers, but rather as modern marine sand bodies. They

observe Sabine and Heald Banks to overlie a ravinement eroding underlying estuarine and tidal

deposits from relict barrier island systems. Therefore, it is possible that these sand bodies are

marine sand bodies reworking relict barrier island material, and established at shoreline positions
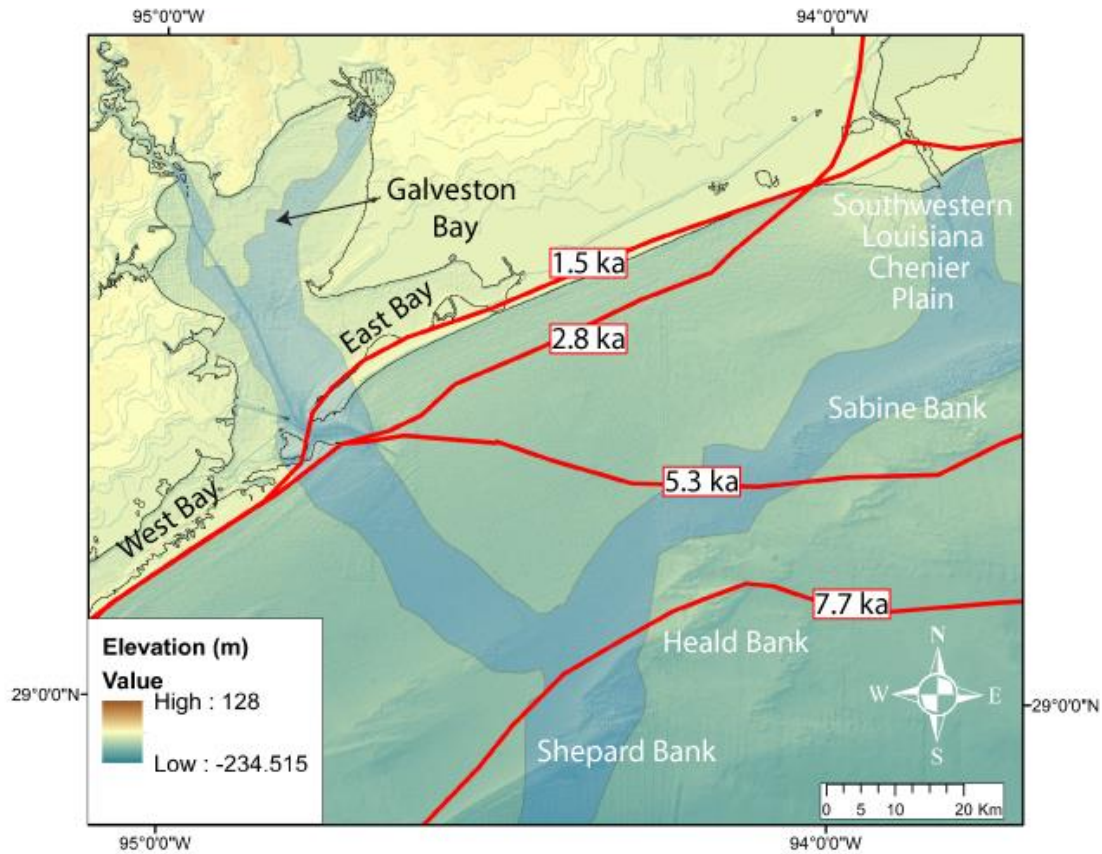
that pre-date the formation of the bank.

Figure 2. Map of the east Texas inner shelf, with the blue polygon representing the Trinity-Sabine incised valley extent (modified from Thomas and Anderson, 1994). Red lines represent paleoshorelines modified from Rodriguez et al., 2004.

3. Methods

3.1 Chirp and 3D Seismic Data

This study utilizes high-resolution chirp sub-bottom reflection data and archived 3D seismic datasets. Over ~ 1000 km of 2D chirp data have been collected by the University of Texas Institute for Geophysics (UTIG) as part of the continuing effort of characterizing offshore sand resources. These data were collected aboard the R/V *Manta* in 2017, the R/V *Brooks McCall* in 2018, and R/V *Trident* in 2018, and consist of 45 profiles parallel to the modern

shoreline ~15 km in length, along with 6 perpendicular profiles ~18 km in length, providing a survey area of ~175 km^2. Chirp data were acquired using an Edgetech 512i sub-bottom profiler towfish configured with a 20 ms, 0.7 to 12 kHz pulse, a 0.0046 ms sample interval, and ~135 ms record length. Full waveform and envelope records were processed in Paradigm Echos software. This workflow includes heave compensation, tide and towfish depth corrections, secondary deconvolution, trace equalization, and a layback correction for navigation (Saustrup et al., 2019). The result of this processing workflow is high-resolution, full waveform data with near decimeter vertical resolution, along with conventional envelope data.

Seismic stratigraphic interpretations were conducted in Landmark DecisionSpace Desktop software. Seismic horizons and units were identified by analyzing a combination of reflection amplitude, configuration, continuity, geometry, and stratigraphic superposition. Approximate depths and thicknesses of seismic horizons and units, respectively, were calculated by converting two-way travel time in milliseconds (ms) to depth in meters below sea level (m) using an average velocity of 1525 m/s (Abdulah et al., 2004).

An archived 3D seismic dataset (B-12-94-TX) was originally acquired commercially in 1994 for geophysical and geological exploration of oil and gas prospects on the U.S. Outer Continental Shelf. Following a 25-year exclusion window, these data were publicly archived by the Bureau of Ocean Energy Management (BOEM) and made available by the United States Geological Survey (USGS) on the National Archive of Marine Seismic Surveys (NAMMS - https://walrus.wr.usgs.gov/namss/). This survey was acquired with a 30 m line spacing, 30 m common depth point spacing, and a 4 ms sampling interval. The processing workflow of these data is not available.

Swartz (2019) retrieved this dataset and conducted further processing steps in Petrel 2016. A crossline filter of 90 m was applied to the data volume in order to smooth striping artifacts resulting from the survey's acquisition footprint. A shallow, regionally conformable horizon located between 40-60 ms interpreted as the base of the Trinity incised valley was mapped and agrees with previous interpretations (Thomas and Anderson, 1994). A 20 ms envelope median coherency attribute was calculated and extracted from this horizon. The result of this median coherency extraction is an amalgamated, time-transgressive representation of the Trinity incised valley fill, highlighting the most anomalous amplitudes within the stratigraphic section.

3.2 Core Data

This study utilizes 2 piston cores, 4 gravity cores, and 1 platform boring to ground-truth seismic datasets. The platform boring was originally collected for foundation studies for drilling rigs and production platforms by Fugro-McClelland Engineers in Houston, which was subsequently reexamined by for lithological and environmental interpretation by Thomas (1991). Gravity cores were collected aboard the R/V *Manta* in 2019, and piston cores were collected aboard the R/V *Brooks McCall* during UTIG's 2018 Marine Geology and Geophysics Field Course. Core sites were selected based on shallow seismic stratigraphic structures observed within seismic data to characterize key transitions within the incised valley fill, evaluate paleoenvironmetal settings, date the transitions from key paleoenvironments, and interpret depositional processes. Thorough detail on the acquisition, processing, and analysis of core data is provided by Standring et al. (2019).
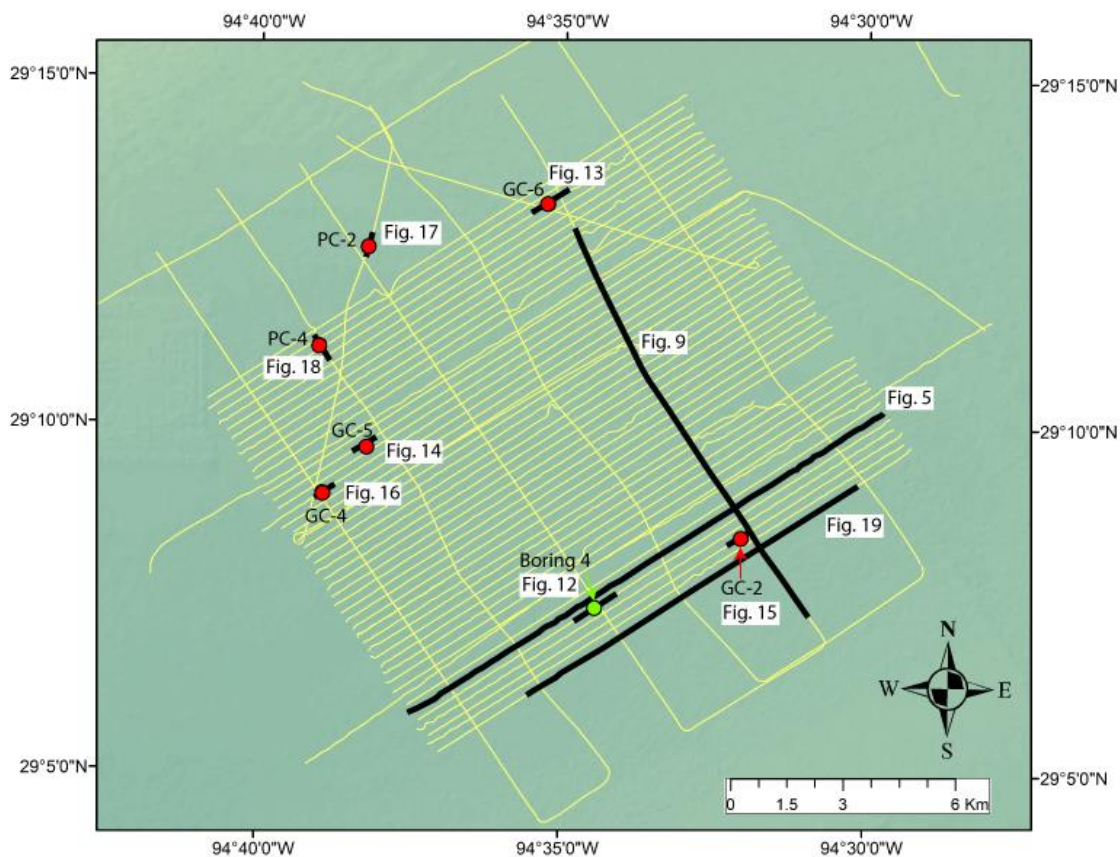
Figure 3. Chirp geophysical tracklines used in this study are represented as yellow lines. Bolded black lines indicate succeeding figure locations used in this study. Red circles represent cores used in Standring et al., 2019 and this study. Green circle represents Boring 4 from Thomas, 1991.

4. Results and Interpretation

Interpretation of chirp data is divided into 5 seismic facies analyzed from full-waveform data (Fig. 4), and 8 seismic horizons that bound 7 seismic units (Figs. 5 – 20) analyzed on both envelope and full-waveform data. Seismic horizons and units are correlated to stratigraphic (Fig. 11), foraminiferal, and radiocarbon data within cores (Figs. 12 – 18) in order to interpret the depositional environment and age of each unit.
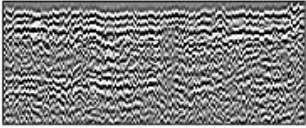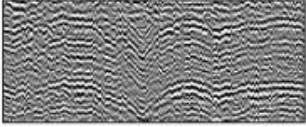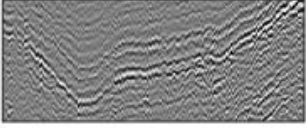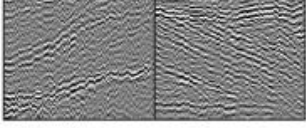
Facies	Example	Description	Units Found In
SF1		Medium-to-high-amplitude, chaotic to discontinuous internal parallel reflections, with some truncations within the facies.	U1, U3, U3b
SF2		Medium-to-high amplitude, U-shaped-to-wavy, parallel, aggrading reflections, with some internal truncations.	U2, U3, U3b
SF3		Low-amplitude, sub-parallel, laminated-to-transparent reflections.	U3, U3a, U4, U5
SF4		Medium-to-low amplitude, draping reflections with internal truncations that depict a cut-and-fill evolution.	U3, U3a
SF5		High-amplitude, unidirectional dipping reflectors that display progradation.	U3, U3b

Figure 4. Seismic facies diagram displaying examples of SF1-5 observed in this study, along with descriptions and the seismic units in which they are found.

4.1 Seismic Facies

We recognize and map five seismic facies throughout the Trinity incised valley fill (Fig. 4), based on reflection amplitude, configuration, continuity, and geometry.

4.1.1 Seismic Facies 1 (SF1)

SF1 (Fig. 4) is composed of medium-to-high-amplitude, chaotic to discontinuous internal parallel reflections, with some internal truncations within the facies. This facies is most commonly observed composing seismic unit U1 (Figs. 6 – 8, 10 – 18, 20), but is also observed within seismic units U3 and U3b (Figs. 10, 11, 15).

4.1.2 Seismic Facies 2 (SF2)

SF2 (Fig. 4) consists of medium-to-high amplitude, U-shaped-to-wavy, parallel, aggrading reflections with some internal truncations. This facies is most commonly associated with seismic unit U2 (Figs. 6 – 17, 22), as well as seismic units U3 and U3b (Figs. 8, 10, 13, 15)

4.1.3 Seismic Facies 3 (SF3)

SF3 (Fig. 4) is characterized by low-amplitude, sub-parallel, laminated-to-transparent reflections. SF3 is frequently found composing seismic unit U4 (Figs. 6 – 8, 10, 12 – 18, 20); however, it is also observed within seismic units U3, U3a (Figs. 12, 17), and U5 (Figs. 6, 8, 17, 20).

4.1.4 Seismic Facies 4 (SF4)

SF4 (Fig. 4) is composed of medium-to-low amplitude, draping reflections with internal truncations that depict a cut-and-fill evolution (e.g., Ronchi et al., 2019). SF4 is found in seismic units U3 and U3a (Figs. 7, 20).

4.1.5 Seismic Facies 5 (SF5)

SF5 (Fig. 4) consists of high-amplitude, unidirectional dipping reflectors that display progradation. SF5 is observed to compose seismic units U3 and U3b (Figs. 8, 11, 15, 20).

4.2 Seismic Horizons

Eight seismic horizons have been mapped bounding characteristic components of the Trinity incised valley fill (Figs. 5 – 20). These surfaces have been defined based on stratigraphic superposition, termination style, and when necessary, associated seismic facies both above and below a given horizon. Time-structure maps were created using a combination of Python and GMT 6 programming scripts, in which horizons were gridded and interpolated onto 50-meter cells (Fig. 21). When appropriate, horizons were converted from two-way travel time in milliseconds to depth in meters below sea level (mbsl) using an average velocity of 1525 m/s (Abdulah et al., 2004).
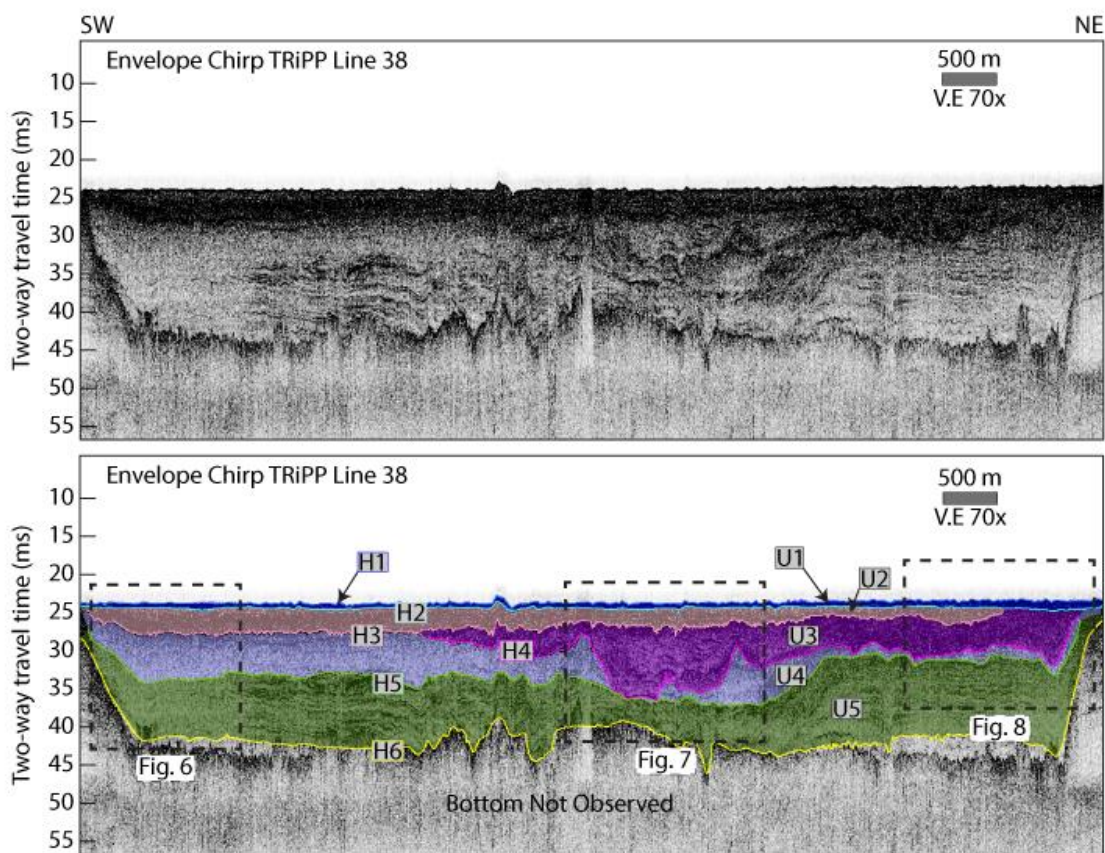

Figure 5. Uninterpreted (top) and interpreted (bottom) envelope chirp data of strike-oriented Tripp Line 38 displaying the seismic horizons (H1-H6) that bound seismic units (U1-U5) within this study. Insets indicate the locations for Figures 6 – 8. The location for this chirp line can be found in Figure 3.
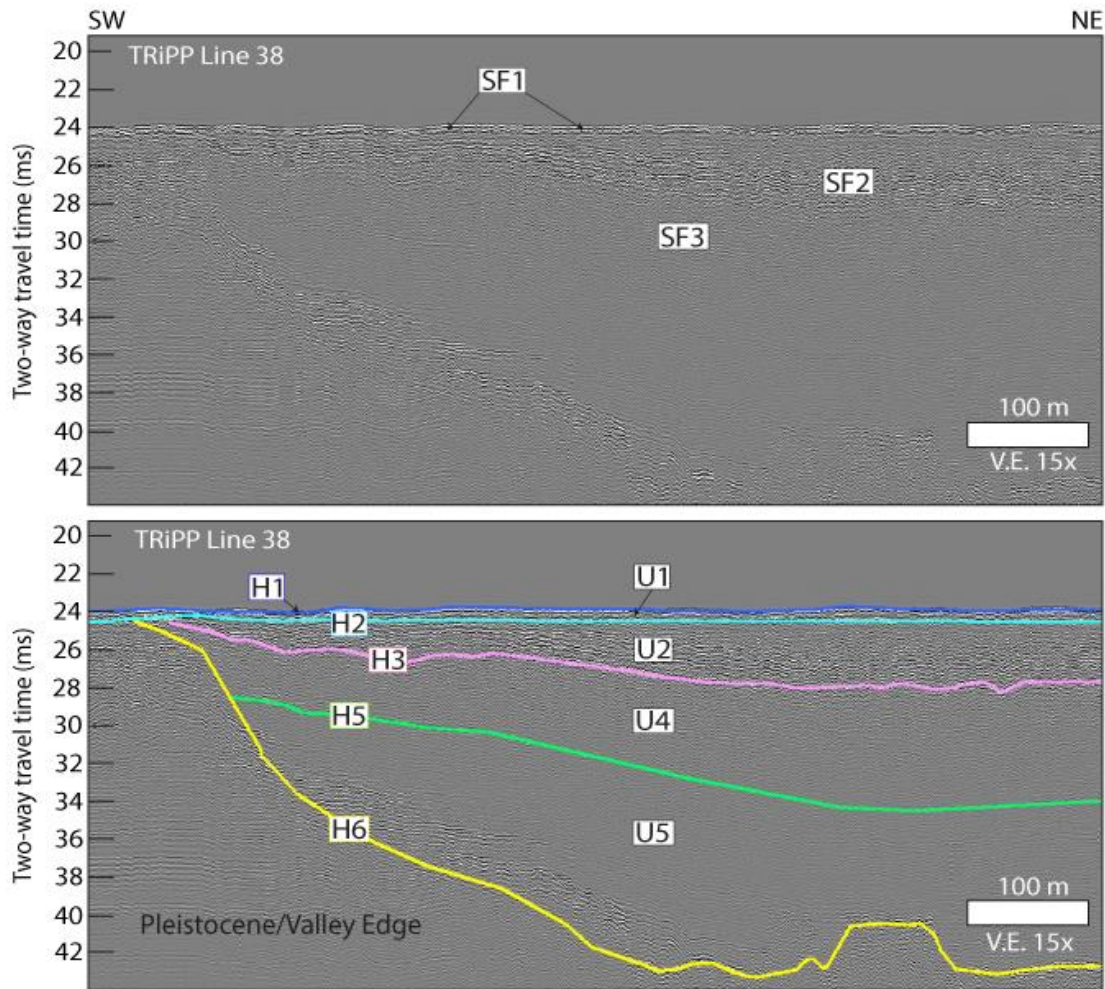
Figure 6. Top – Seismic facies analysis of full-waveform data on Tripp Line 38. Bottom – Interpretation of full-waveform data on Tripp Line 38. Displayed here is the western edge of the Trinity incised valley, defined by H6. Seismic units U5, U4, and U2, bound by seismic horizons H6, H5, and H3, are seen either onlapping the valley wall, or truncated by H2. H1 represents the seafloor. The location for this chirp line can be found on Figures 3 and 5.
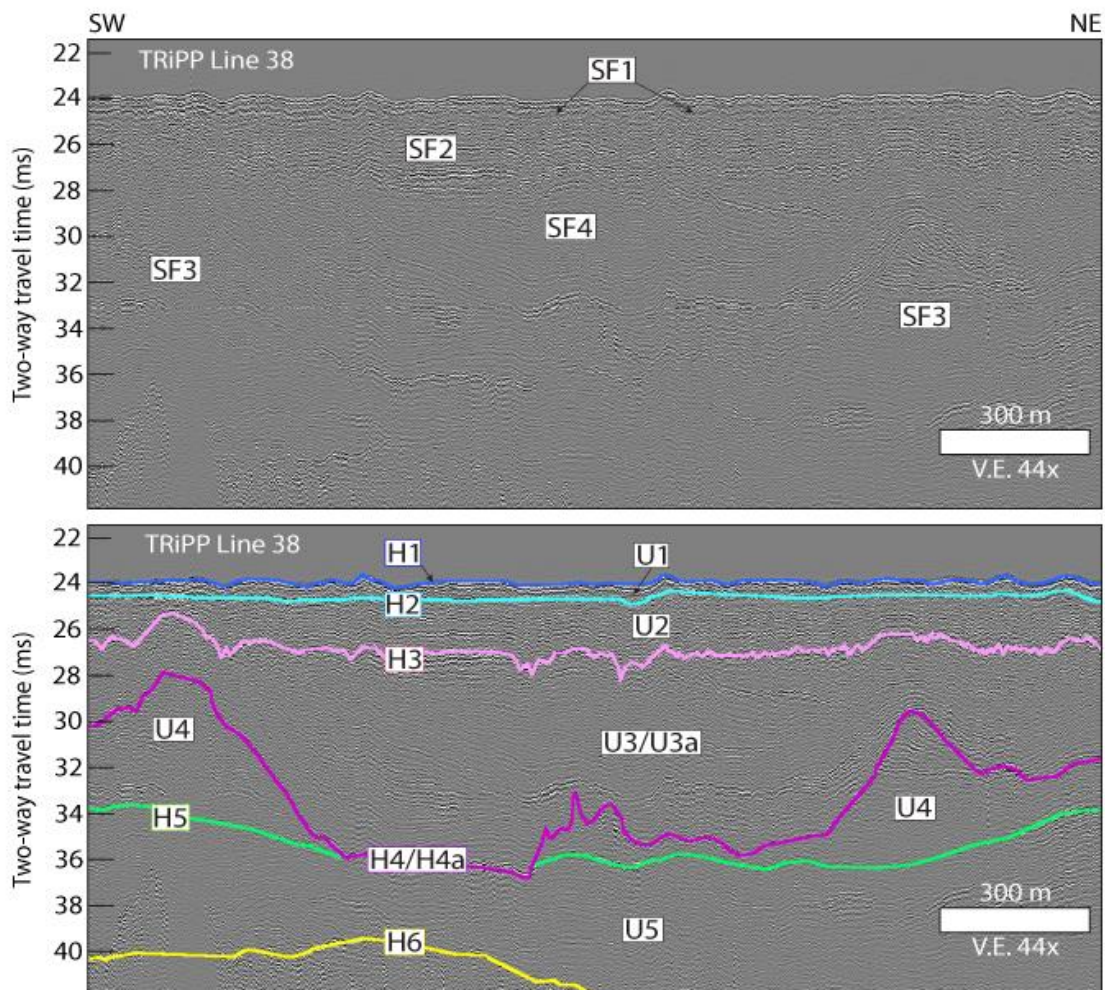
Figure 7. Top – Seismic facies analysis of full-waveform data on Tripp Line 38. Bottom – Interpretation of full-waveform data on Tripp Line 38. Displayed here is the central portion of the Trinity incised valley. H6 is shown in the bottom of the figure as a channelized, continuous reflector. H5, defining the top of U5, is truncated by overlying horizons. H4/H4a, which forms the lower bound of U3/U3a, is composed of SF4. Horizons H3 and H2 bound unit U2. H1 is the seafloor. The location for this chirp line can be found on Figures 3 and 5.

Figure 8. Top – Seismic facies analysis of full-waveform data on Tripp Line 38. Bottom – Interpretation of full-waveform data on Tripp Line 38. Displayed here is the eastern portion of the Trinity incised valley. H6 is shown on the right to define the incised valley edge. H5, defining the top of U5, is truncated H4/H4b. H4/H4b, which forms the lower bound of U3/U3b, is composed of SF2 and SF5. Horizons H3 and H2 bound unit U2. H1 is the seafloor. The location for this chirp line can be found on Figures 3 and 5.
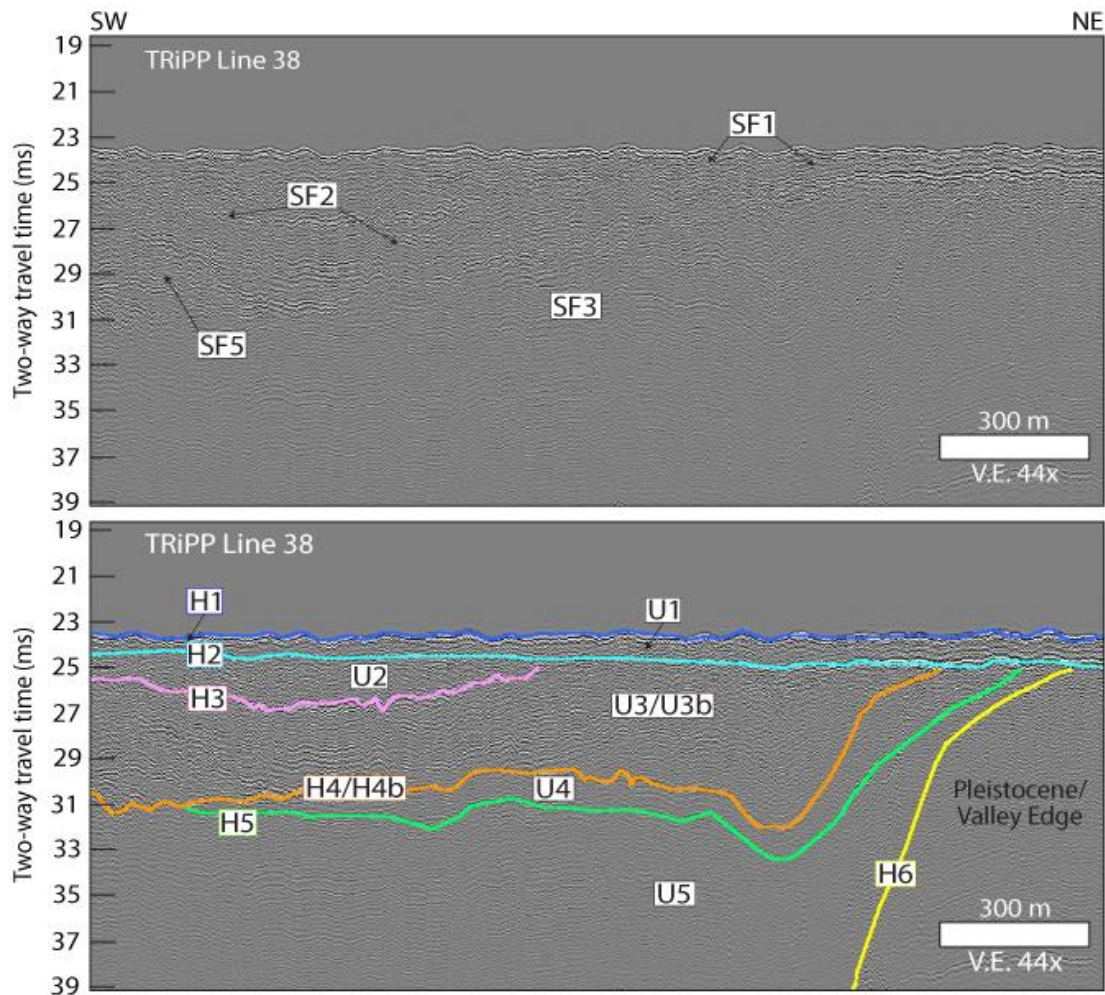
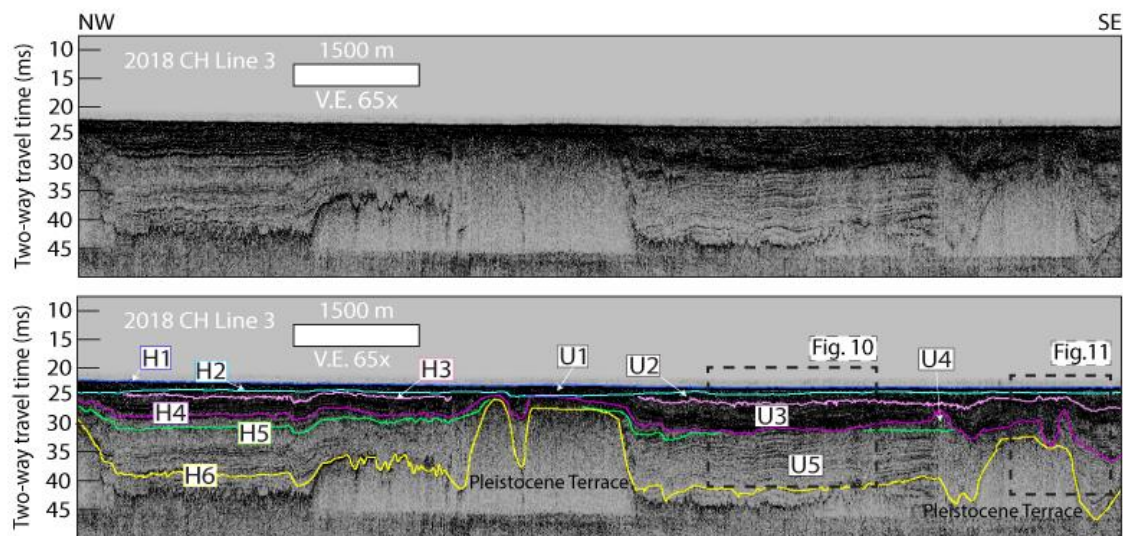Figure 9: Uninterpreted (top) and interpreted (bottom) envelope chirp data of the dip-oriented 2018 CH Line 3 displaying the seismic horizons (H1-H6) that bound seismic units (U1-U5) within this study. Channels initiated by H6 are propagated throughout the overlying stratigraphic section. Insets indicate the locations for Figures 10 and 11. The location for this chirp line can be found in Figure 3.

Figure 10: Top – Seismic facies analysis of full-waveform data on 2018 CH Line 3. Bottom – Interpretation of full-waveform data on 2018 CH Line 3. Displayed here is a dip-oriented line, highlighting the truncation of H5 by H4/H4b. U3/U3b, in which H4/H4b represents its lower boundary, is composed of SF1 and SF2 in the form chaotic-to-discontinuous reflections and U-shaped, aggrading reflections, respectively. Horizons H3 and H2 bound unit U2. H1 is the seafloor. The location for this chirp line can be found on Figures 3 and 9.
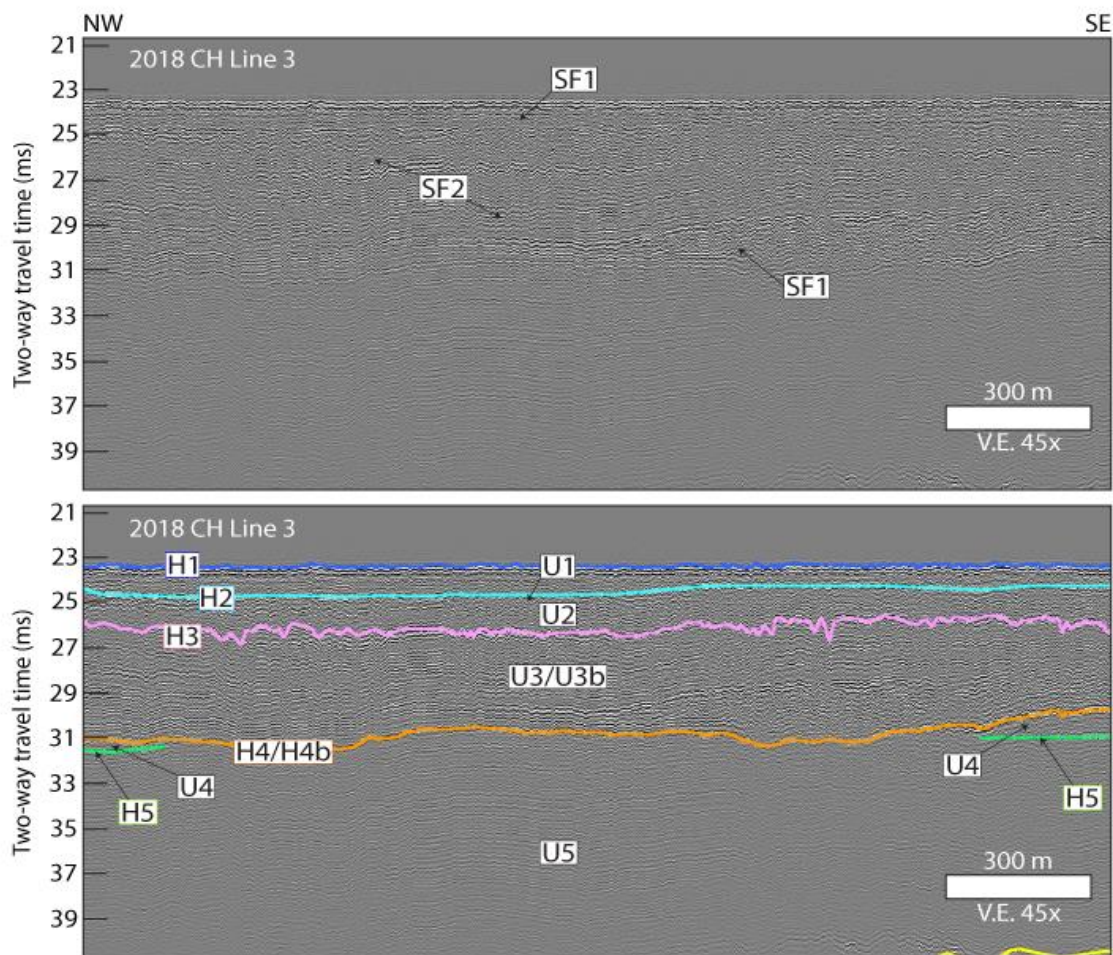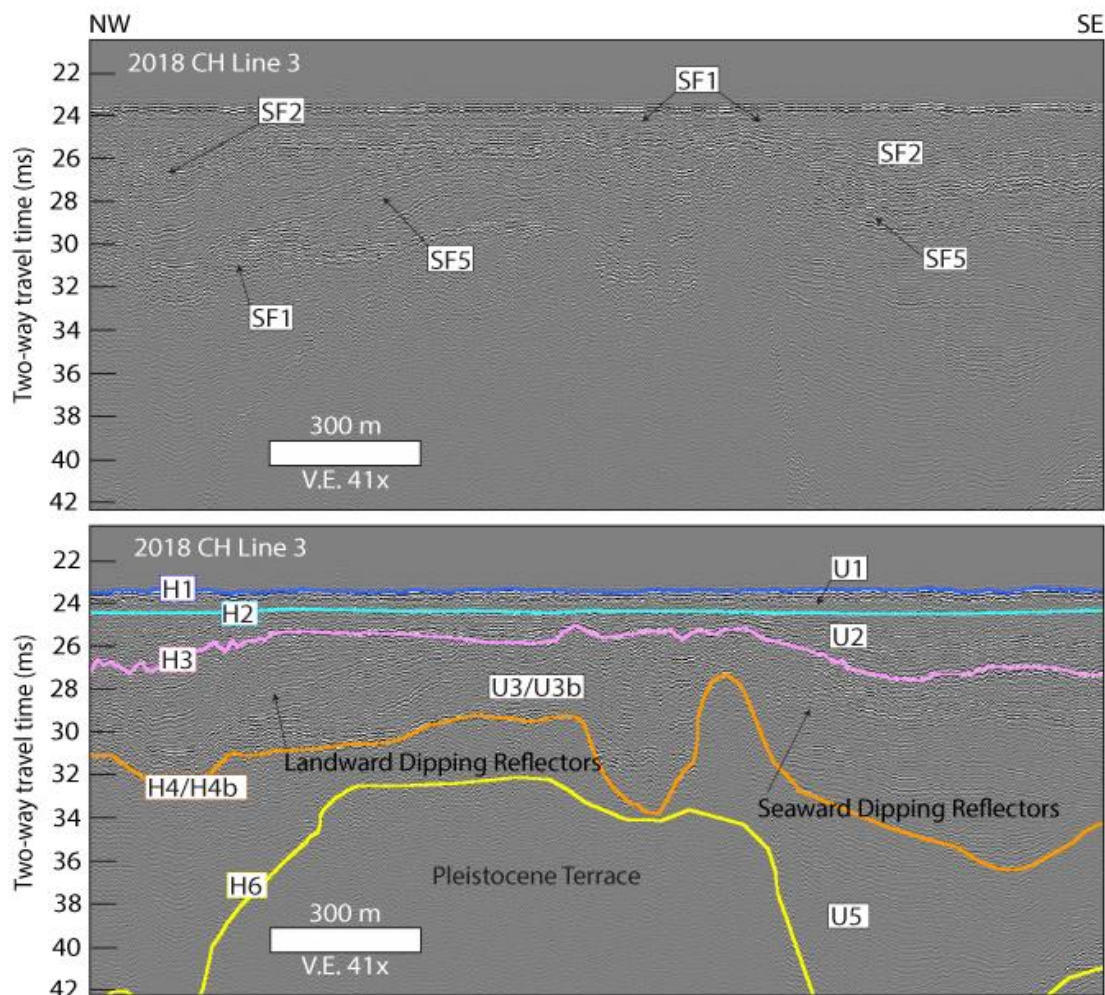
Figure 11: Top – Seismic facies analysis of full-waveform data on 2018 CH Line 3. Bottom – Interpretation of full-waveform data on 2018 CH Line 3. Displayed here is the seaward most extent of a dip-oriented line. H6 is shown as a mound-like feature interpreted as a Pleistocene fluvial terrace, overlain by U5. U3/U3b, which lies above H4/H4b, is composed of SF1 and SF5, and displays a transition from landward dipping reflectors to seaward dipping reflectors, indicating proximal paleo-barrier position over the Pleistocene fluvial terrace. H3 bounds U2, which is composed of SF2, and is truncated by the overlying H2 horizon. H1 is the seafloor. The location for this chirp line can be found on Figures 3 and 9.

4.2.1 Horizon H1

H1 is the modern seafloor, which displays a general southwestward dip (Fig. 21 – H1). H1 is shallowest within the northeastern portion of the study area at 19 ms depth (~14.5 mbsl) and deepest within the southwestward portion at 25 ms depth (~19 mbsl). This horizon is often erosional in nature, and frequently amalgamates with the underlying H2 horizon (Figs. 5 – 7, 12, 14, 16, 17).

4.2.2 Horizon H2

H2 is a varying amplitude erosional surface that truncates underlying reflectors (Fig. 21 – H2), and varies between 20 and 26 ms depth (~15 and 20 mbsl). Frequently, this horizon amalgamates with the overlying H1 horizon and mimics underlying topography (Figs. 5 – 7, 12, 14, 16, 17). This horizon is erosional in nature, where it is observed to truncate underlying strata in the form of multiple 2-4.5 km long, 1.3- 1.5 km wide, 0.75- 2.8 ms (~1 to 2 m) deep channel-like features (Figs. 8, 13, 21). Due to its truncation of underlying reflectors (Figs. 6, 8, 9, 13, 16, 19), and its correlation beneath a transgressive lag in core GC-6 (Fig. 13), this horizon is interpreted to be the transgressive ravinement, which is a diachronous surface cut during the process of erosional shoreface retreat (e.g. Nummendal and Swift, 1987) that has been subsequently reworked by the modern seafloor.

4.2.3 Horizon H3

H3 is a high-amplitude, channelized, erosional surface that truncates underlying strata, and varies between 23 and 30 ms depth (~17.5 and 23 mbsl) (Fig. 21 – H3). This horizon is truncated by the overlying H2 horizon (Figs. 5, 6, 8, 9, 13, 16, 19). H3 is deepest and appears most continuous along the western and seaward portions of the study area (Figs. 5 – 7, 9 – 12, 14

– 17, 19 – 21). Conversely, this horizon is shallowest and least continuous along the eastern and landward portions of the study area (Figs. 5, 8, 9, 13, 21), or above fluvial terraces (Fig. 18). Based on foraminiferal analyses (Standring et al., 2019), H3 is interpreted to be the base of (Figs. 14 – 18) or lie within (Fig. 13) outer bay sediments, a high-energy environment just landward of ancient barriers formed by tidal, storm, and wave processes (Dalrymple et al., 1992; Zaitlin et al., 1994).

4.2.4 Horizon H4

H4 is a varying amplitude, highly erosional surface that truncates the underlying H5 horizon (Figs. 5, 7 – 10, 15, 19, 20) and varies between 22 and 44 ms depth (~16.5 to 33.5 mbsl) (Fig. 21 – H4). This horizon is subsequently truncated either by H3 along the western portion of study area (Figs. 5, 19) or H2 along the eastern portion (Figs. 5, 8, 9, 19). H4 is deepest within the seaward portion of the study area, defining an approximately 3.5 to 5 km wide channel that rapidly shallows landward (Fig. 21 – H4). Due to its erosional nature and channelized geometry (Figs. 5, 7 – 11, 13, 15, 19 – 21), the horizon is interpreted as a tidal ravinement (e.g. Cattaneo and Steel, 2003) formed in a high-tidal-energy environment adjacent to or just landward of the barrier (Dalrymple et al., 1992; Zaitlin et al., 1994). H4 is divided into two sub-horizons H4a and H4b based on seismic facies characterizations of SF4 and SF5 overlying them, respectively (Figs. 7, 8, 10, 11, 15, 20).

4.2.5 Horizon H4a

H4a is varying amplitude, deeply channelized, highly erosional surface that truncates the underlying H5 horizon (Figs. 7, 20) and is truncated by the overlying H3 horizon (Figs. 5, 19).

H4a varies between 22 and 44 ms (~16.5 to 33.5 mbsl) (Fig. 21 – H4a). This horizon is distinct

from H4b due to the presence of seismic facies SF4 overlying it (Figs. 7, 20). H4a displays a

highly erosional channel approximately 2 km wide at its maximum extent (Fig. 21 – H4a). Deep

erosional cuts made by this horizon are focused within the seaward extent of the study area (Figs.

7, 20), which quickly shallows landward and along the channel margins (Figs. 5, 9, 17, 19, 21).

Based on its highly erosional nature, stratigraphic superposition, and overlying seismic facies,

H4a is interpreted to be the base of a paleo-tidal inlet (e.g., Storms et al., 2008; Ronchi et al.,

2018; Ronchi et al., 2019).

4.2.6 Horizon H4b

H4b is a varying amplitude, shallowly channelized, highly erosional surface that

truncates the H5 horizon (Figs. 8, 10, 15, 20), and is truncated by the overlying H2 horizon (Fig.

8). H4b varies between 22 and 37 ms depth (~16.5 and 28 mbsl) (Fig. 21 – H4b). This horizon is

differentiated from H4a by having seismic facies SF5 overlying it (Figs. 8, 11, 15, 20).

Additionally, H4b reaches shallower depths than H4a (~5.5 m difference) and is focused along

the eastern portion of the study area (Figs. 8, 10, 11, 13, 15, 19, 20). Given this horizon's highly

erosional nature, stratigraphic superposition, and overlying seismic facies, H4b is interpreted as

the base of a paleo-tidal delta (e.g., Rodriguez et al., 1998).

4.2.7 Horizon H5

H5 is a varying amplitude reflection that onlaps the incised valley walls (Figs. 5, 6, 19) or

is truncated by H2 along the valley margins (Figs. 5, 8, 16). This horizon varies between 23 and

37 ms depth (~17.5 and 28 mbsl). (Fig. 21 – H5). H5 is extensive throughout most of the study

area, but frequently truncated by H4, H4a, and H4b within the seaward portion of the study area (Figs. 7 – 10, 15, 19, 20), resulting in holes within the H5 horizon time-structure map (Fig. 21 – H5). This horizon is deepest within the seaward portion of the study area, reaching its maximum depth of 37 ms (~28 mbsl) within a 2 km wide channelized feature (Fig. 21 – H5). H5 then rapidly shallows toward the valley margins and the landward portion of the study area (Fig. 21 – H5). H5 has been previously interpreted as the boundary between underlying deltaic or upper-bay sediments and overlying bay sediments (Thomas, 1991; Swartz, 2019).

4.2.8 Horizon H6

H6 is a low-to-high-amplitude planar to rugose reflection (Figs. 5 – 9, 11, 12, 16 – 19). This horizon varies between 19 ms depth (~14.5 mbsl) and 50 ms depth (~38 mbsl) (Fig. 21 – H6). Along the edges of the valley, H6 truncates strata lying outside the valley, while strata within the valley onlap this surface (Fig. 6, 8, 16). This horizon has been previously interpreted as a sharp acoustic and sedimentological boundary between underlying fluvial sediments and overlying deltaic sediments (Figure 12; Thomas 1991; Thomas et al., 1994; Swartz, 2019).

4.3 Seismic Units

Seven seismic units are bound by these eight upper and lower seismic horizons (Figs. 5 – 20). The units have been characterized by bounding surface stratigraphic position and seismic facies association, and ground-truthed by stratigraphic and foraminiferal core data (Figs. 12 – 18). Time-thickness maps, or isopachs, were created using a combination of Python and GMT 6 programming scripts by differencing the two-way travel time for bottom and top boundaries of the identified seismic unit, and then gridding and interpolating these values onto 50-meter cells

(Fig. 22). Seismic units were converted from two-way travel time in milliseconds to thickness in meters using an average velocity through unconsolidated sand/mud of 1525 m/s (Abdulah et al., 2004).

Figure 12. Top – Seismic facies analysis of full-waveform data on Tripp Line 39. Bottom – Interpretation of full-waveform data on Tripp Line 39. Displayed here is a strike-oriented line, which is tied to Boring 4 from Thomas, 1991, and modified from Swartz, 2019. Paleoenvironmental shifts interpreted by Thomas, 1991 are correlated to seismic stratigraphy. U5, U4, U3/U3a, U2, and U1 are bound by horizons H6, H5, H4/H4a, H3, H2, and H1. The location for this chirp line can be found on Figure 3.

Figure 13. Top – Seismic facies analysis of full-waveform data on Tripp Line 2. Bottom – Interpretation of full-waveform data on Tripp Line 2. Displayed here is a strike-oriented line, which is tied to gravity core GC-6 modified by Standring et al., 2019. The core description provides lithologic information, along with radiocarbon dates (small black text and stars), age models (small green text), and paleoenvironmental interpretations. Horizons that are penetrated by the core are displayed as colored lines. The location for this chirp line can be found on Figure 3.
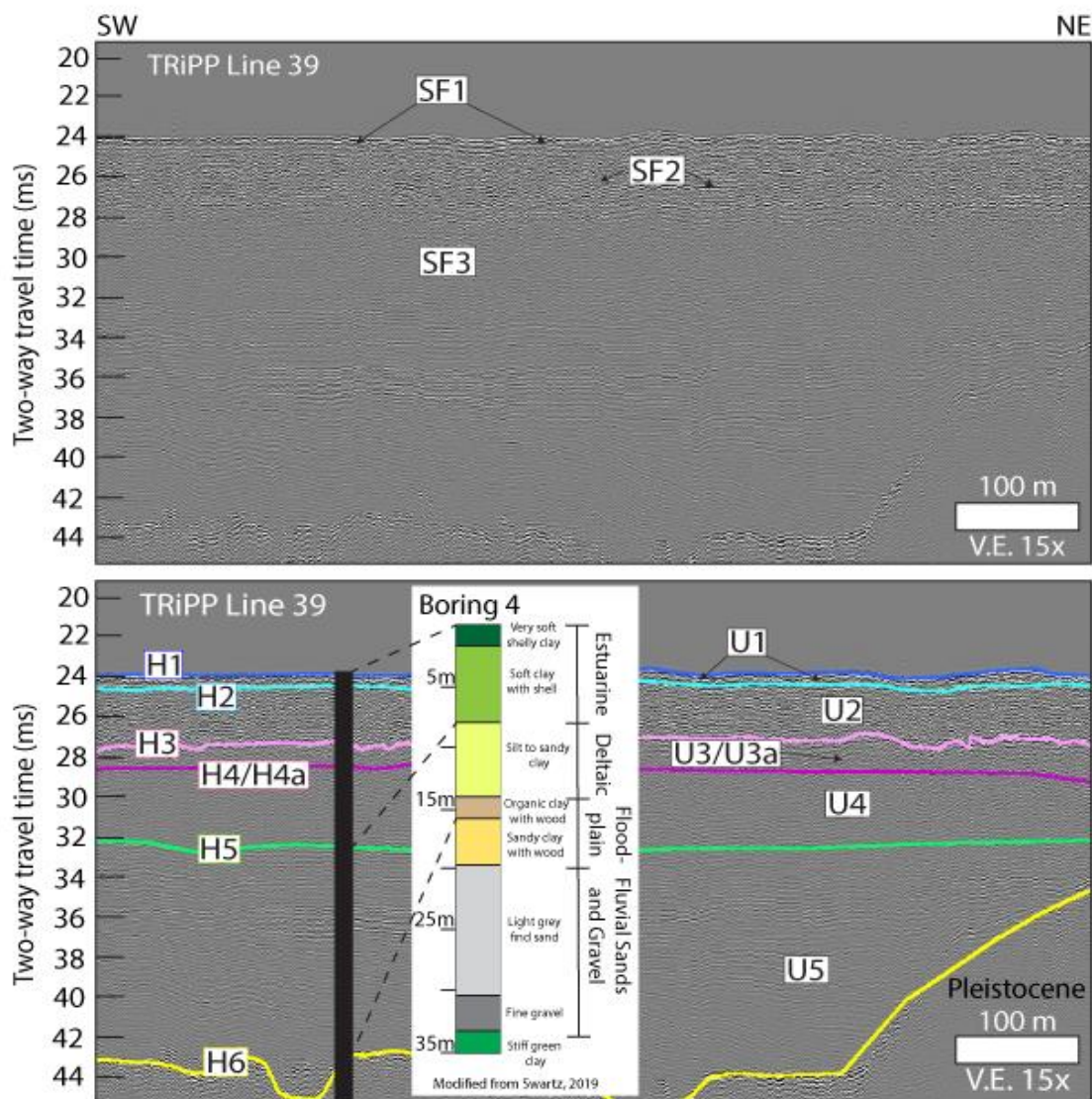
Figure 14. Top – Seismic facies analysis of full-waveform data on Tripp Line 13. Bottom – Interpretation of full-waveform data on Tripp Line 13. Displayed here is a strike-oriented line, which is tied to gravity core GC-5 modified by Standring et al., 2019. The core description provides lithologic information, along with radiocarbon dates (small black text and stars), age models (small green text), and paleoenvironmental interpretations. Horizons that are penetrated by the core are displayed as colored lines. The location for this chirp line can be found on Figure 3.
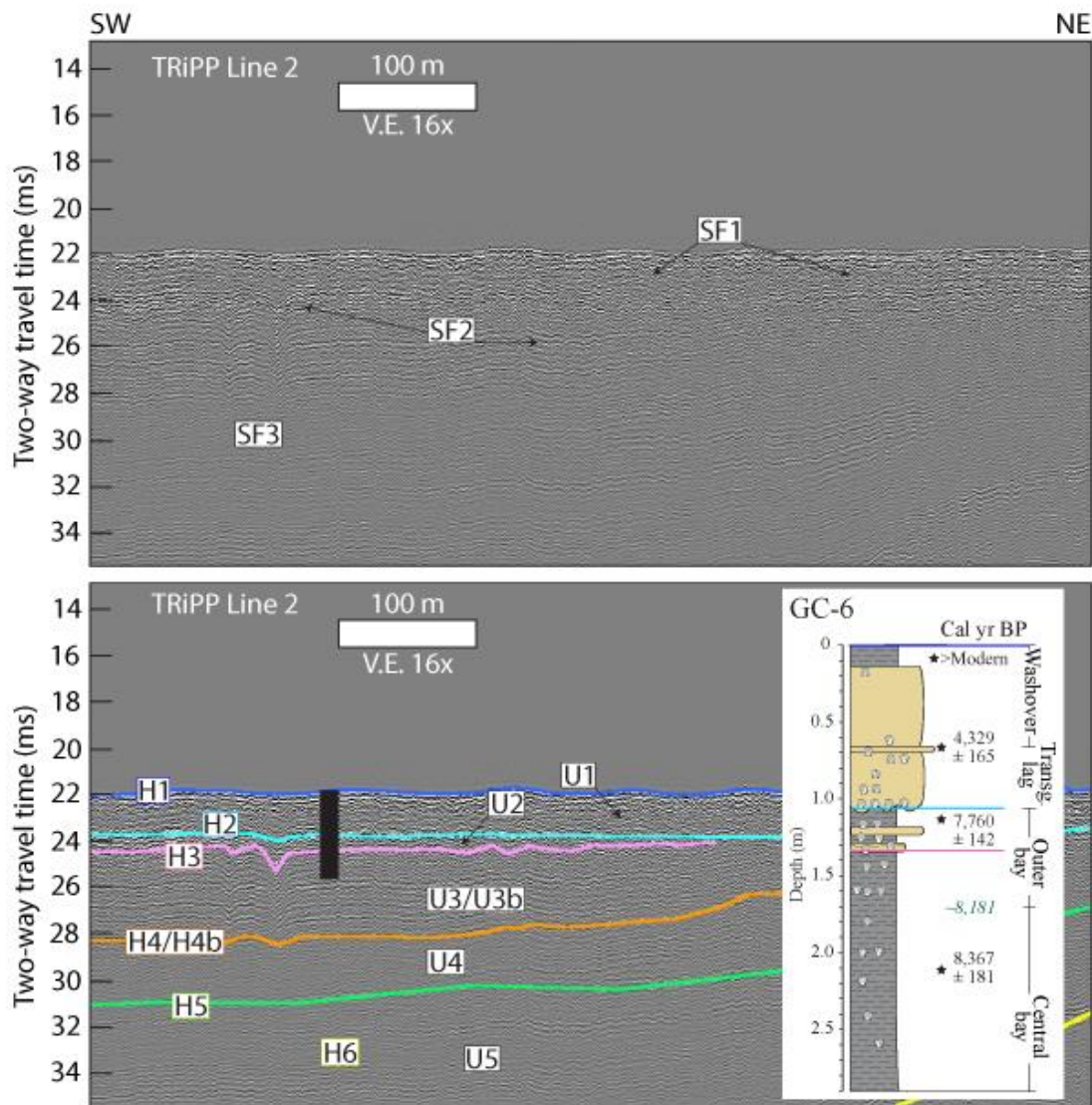
Figure 15: Top – Seismic facies analysis of full-waveform data on Tripp Line 41. Bottom – Interpretation of full-waveform data on Tripp Line 41. Displayed here is a strike-oriented line, which is tied to gravity core GC-2 modified by Standring et al., 2019. The core description provides lithologic information, along with radiocarbon dates (small black text and stars), age models (small green text), and paleoenvironmental interpretations. Horizons that are penetrated by the core are displayed as colored lines. The location for this chirp line can be found on Figure 3.
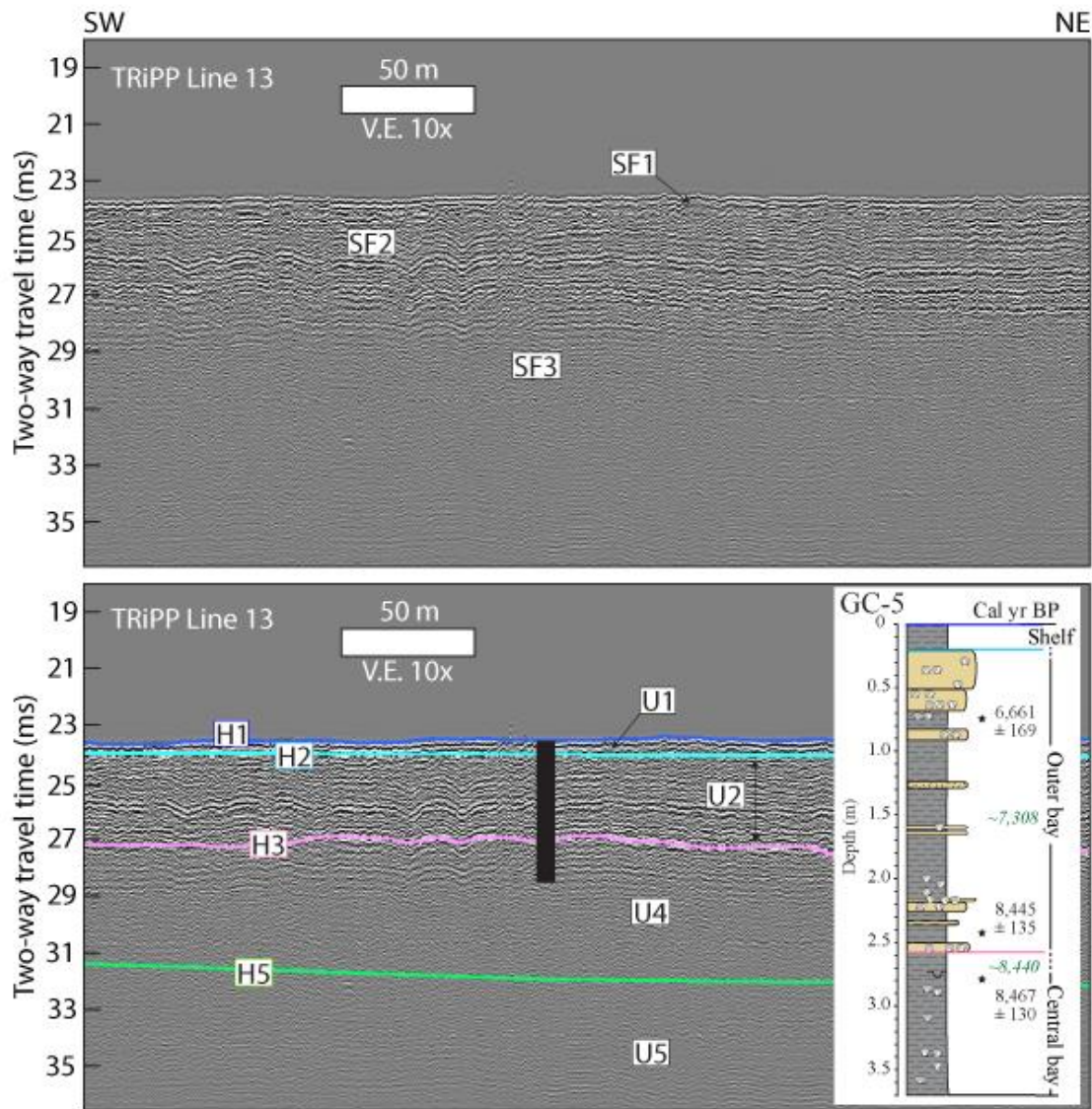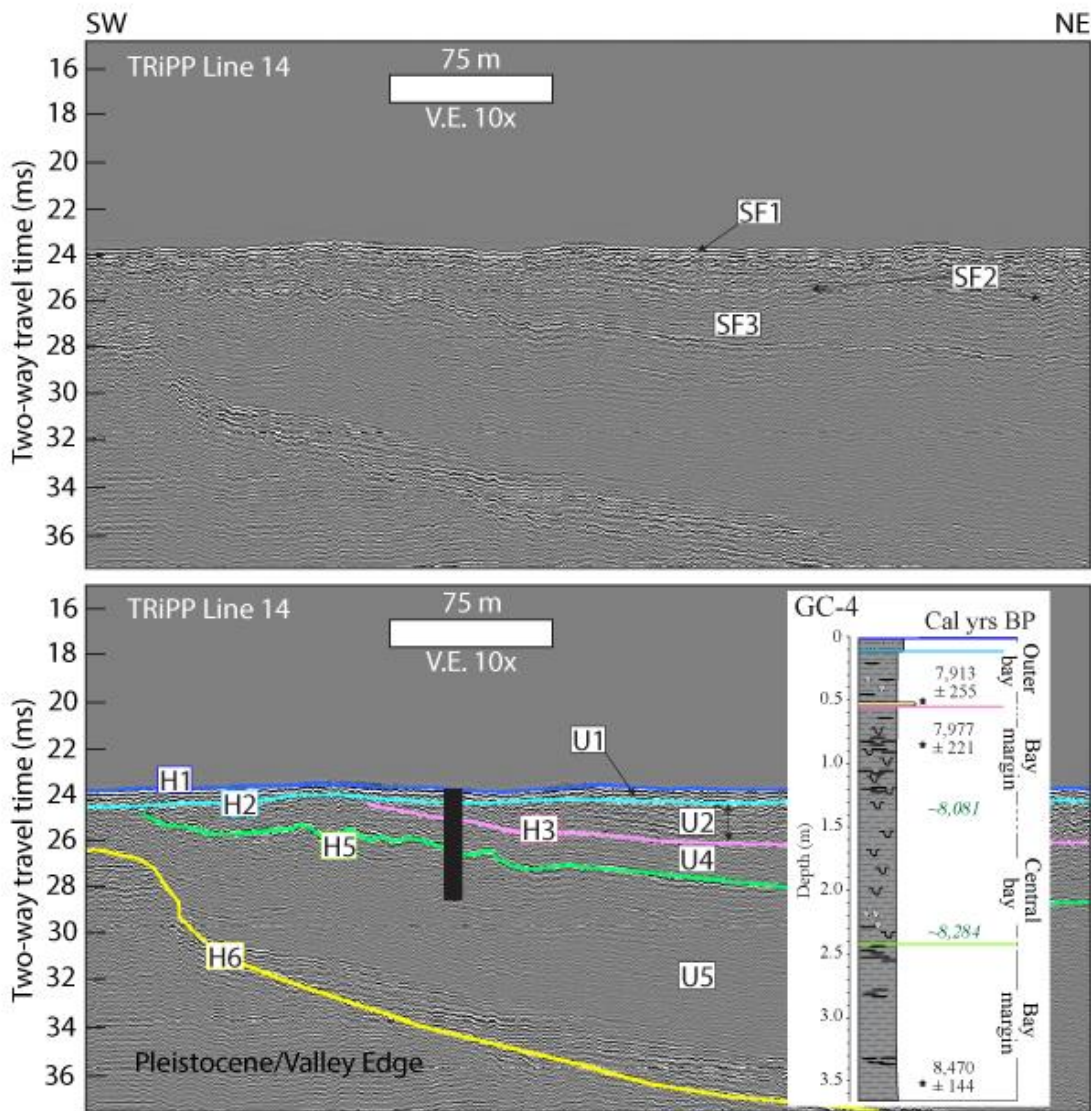
Figure 16: Top – Seismic facies analysis of full-waveform data on Tripp Line 14. Bottom – Interpretation of full-waveform data on Tripp Line 14. Displayed here is a strike-oriented line, which is tied to gravity core GC-4 modified by Standring et al., 2019. The core description provides lithologic information, along with radiocarbon dates (small black text and stars), age models (small green text), and paleoenvironmental interpretations. Horizons that are penetrated by the core are displayed as colored lines. The location for this chirp line can be found on Figure 3.
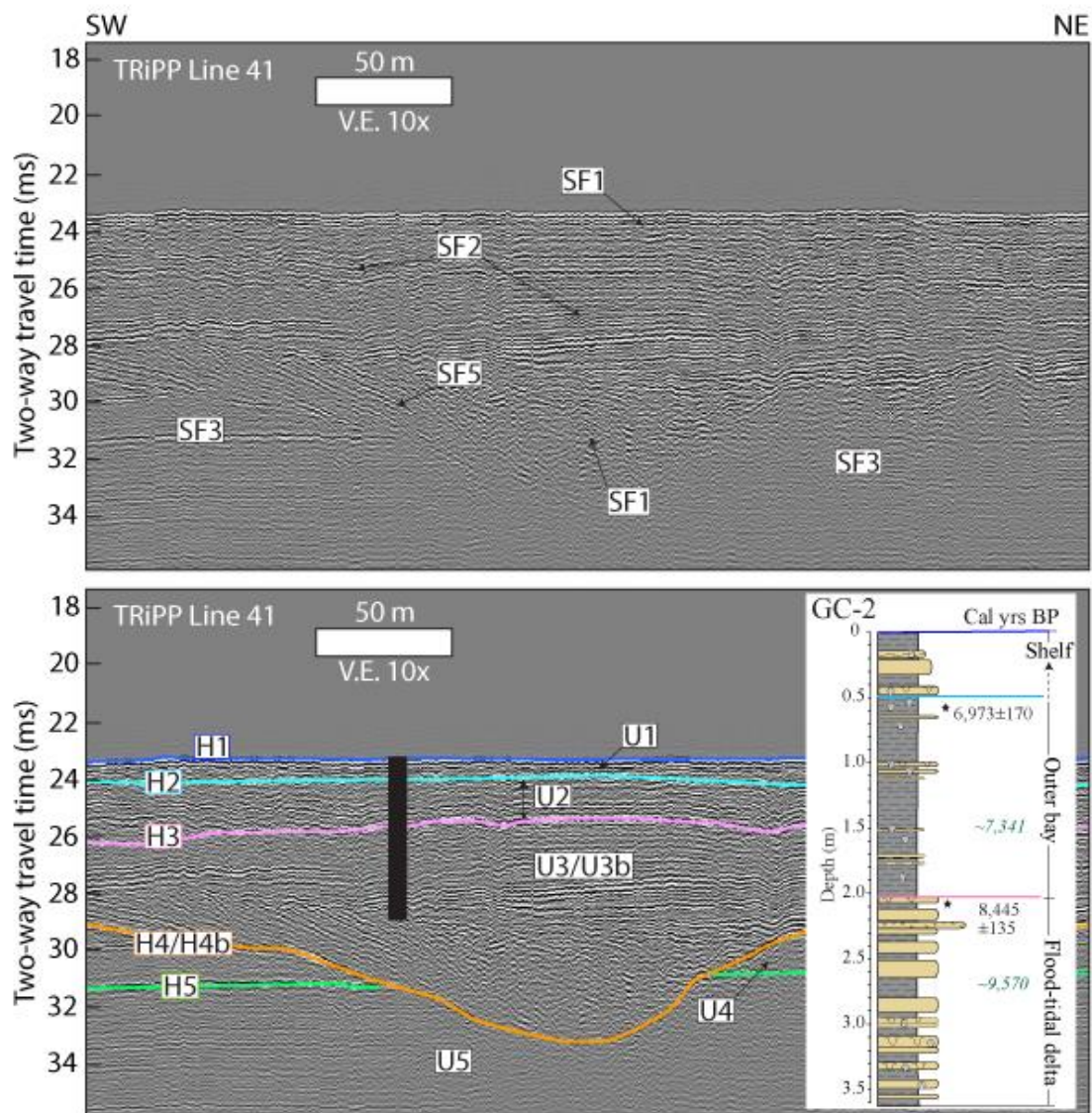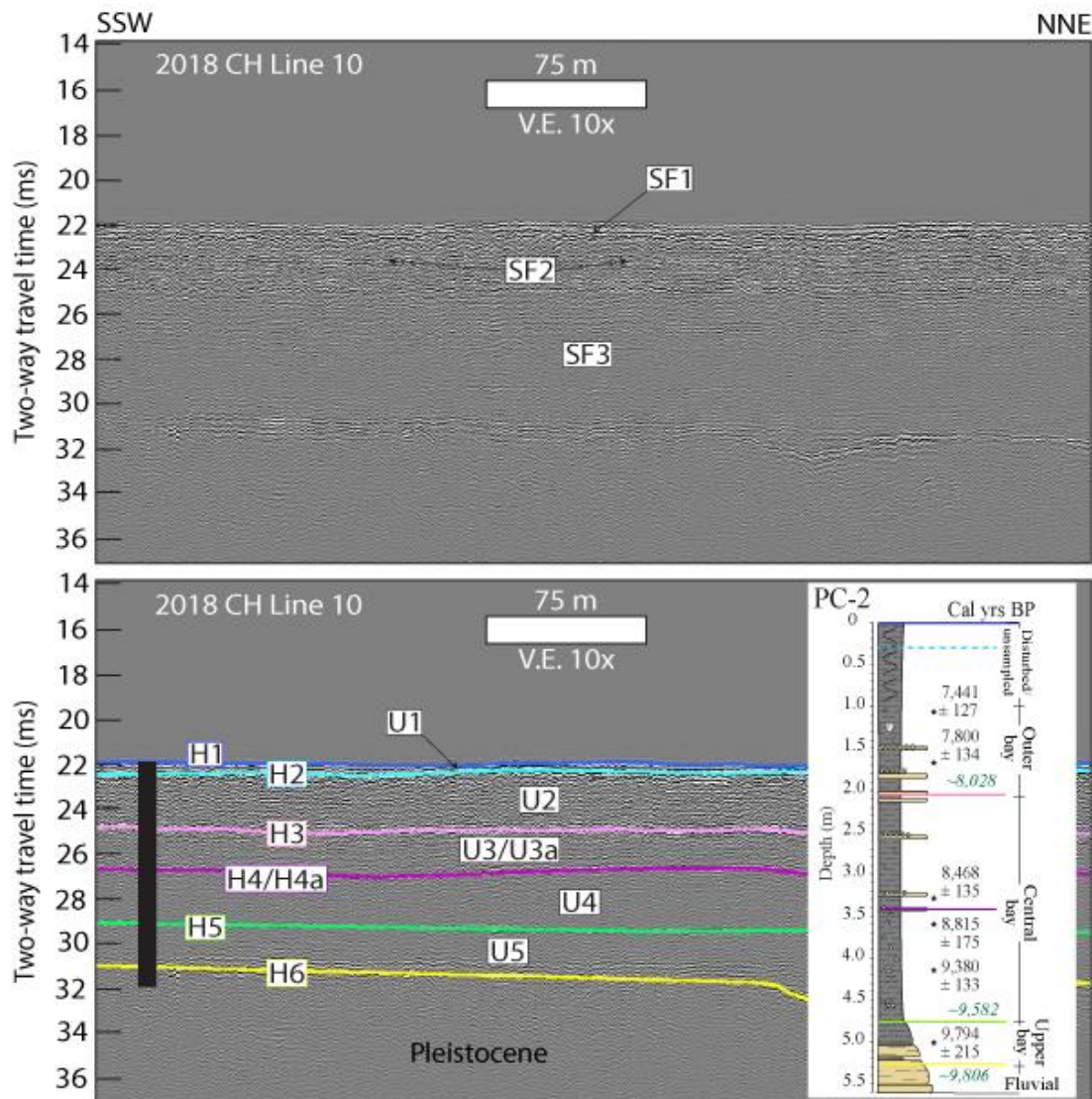
Figure 17: Top – Seismic facies analysis of full-waveform data on 2018 CH Line 10. Bottom – Interpretation of full-waveform data on 2018 CH Line 10. Displayed here is a dip-oriented line, which is tied to piston core PC-2 modified by Standring et al., 2019. The core description provides lithologic information, along with radiocarbon dates (small black text and stars), age models (small green text), and paleoenvironmental interpretations. Horizons that are penetrated by the core are displayed as colored lines. The location for this chirp line can be found on Figure 3.

Figure 18: Top – Seismic facies analysis of full-waveform data on 2018 CH Line 10. Bottom – Interpretation of full-waveform data on 2018 CH Line 17. Displayed here is a dip-oriented line, which is tied to piston core PC-4 modified by Standring et al., 2019. The core description provides lithologic information, along with radiocarbon dates (small black text and stars), age models (small green text), and paleoenvironmental interpretations. Horizons that are penetrated by the core are displayed as colored lines. The location for this chirp line can be found on Figure 3.
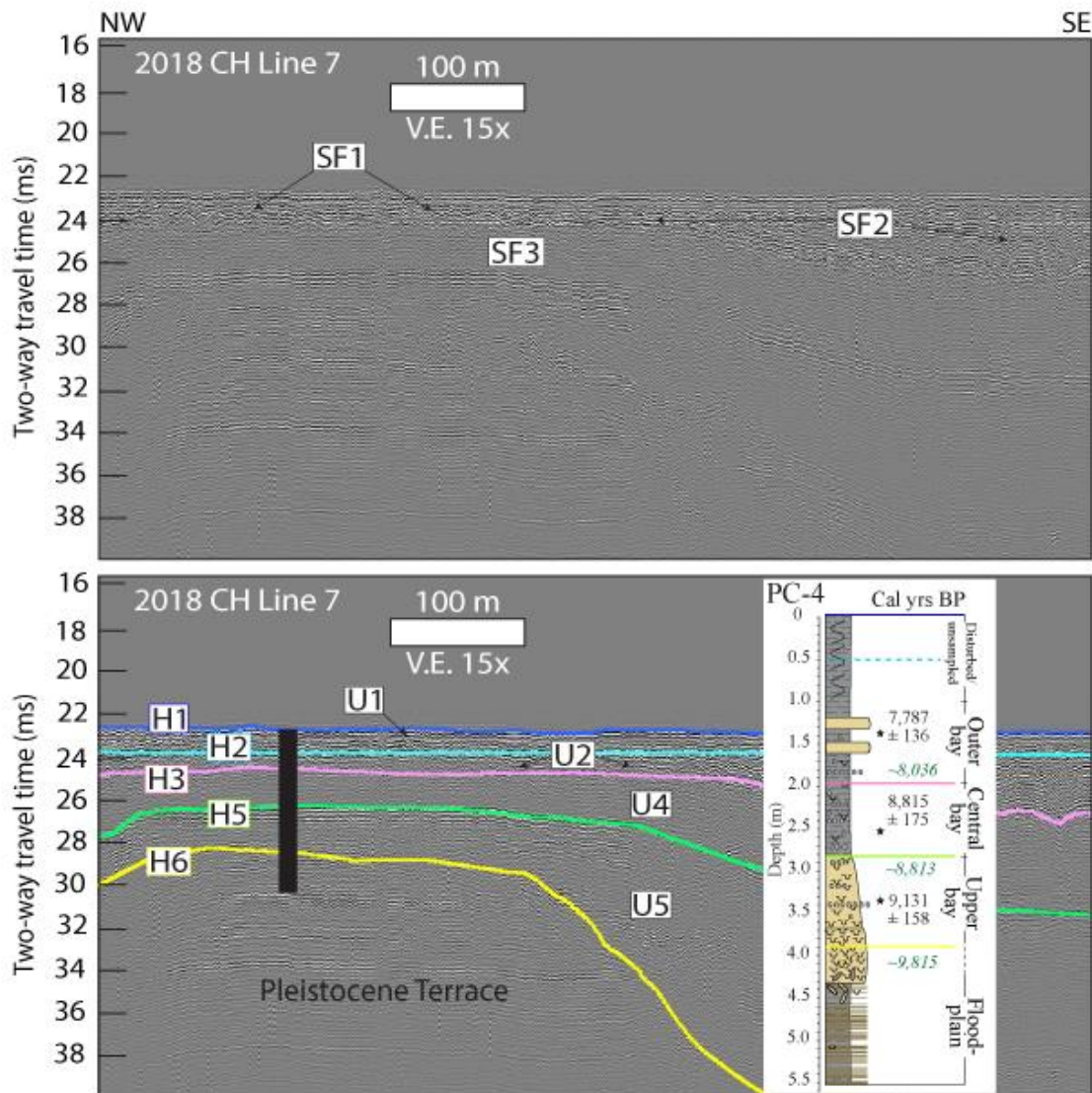
4.3.1 Unit 1 – Transgressive Deposits (U1)

U1 is has an upper boundary of H1, a lower boundary of H2, and is composed of SF1 (Figs. 5 – 20). This unit ranges in thickness from 0 to 2.8 ms (~0 to 2 m) (Fig. 22 – U1), and is unique in that it is the only unit in this study to have been deposited beyond the valley walls. Sediments cored from this unit vary from uncompacted, "soupy" sediments (Figs. 14, 16 – 18), to coarser-grained sediments (Figs. 13, 15). U1 is generally thinnest along the western portion of the study area, where its lower bounding horizon U2 amalgamates near or directly with the seafloor, and corresponds to disturbed core samples due to uncompacted sediment (Figs. 17, 18). Where U1 is better preserved in flat-lying regions, foraminiferal data, which display an overall increase in diversity (Standring et al., 2019), reveal U1 is likely derived from an inner shelf environment (Figs. 14, 15).

This unit reaches its greatest thickness along the eastern portion of the study area where it infills deep channel-like features formed by the horizon H2 (Figs. 13, 21, 22). Sediment cored from the margin of the largest of such channel-like features shows U1 to be composed of an ~0.8 m package of sandy sediments (Fig. 13). This coarse-grained package overlies horizon H2, which is observed to truncate the underlying H3 horizon (Fig. 13). Foraminiferal analysis of this isolated package reveal U1 is likely composed of one or multiple washover deposits overlying an erosive transgressive lag deposit (Fig. 13; Standring et al., 2019).

Dating this unit is difficult due to the removal of material above the transgressive ravinement, apart from a single radiocarbon date taken from a mollusk shell dated to ~4.3 ka (Figure 13; Standring et al., 2019). However, age models performed on environmental transitions indicate that the paleo-estuary likely transitioned to an inner shelf environment by ~6.9 ka (Standring et al., 2019). Therefore, U1 is interpreted as a time-transgressive, patchy veneer of sediment composed of either uncompacted fine-grained material derived from an inner shelf environment,

or ~2m thick coarse-grained package composed of washover deposits and transgressive lags derived from a relict barrier, forming at least by ~6.9 ka, and persisting through ~4.3 ka. These unconsolidated muds, sands, and shells are interpreted to be associated with the transgressive ravinement, reworking underlying material over a span of ~2.6 kyr (Nummendal and Swift, 1987; Swift and Thorn, 1991; Cattaneo and Steel, 2003).

4.3.2 Unit 2 – Outer Bay (U2)

U2 has an upper boundary of H2, a lower boundary of H3, and is composed of SF2 (Figs. 5 – 20). This unit ranges in thickness from ~0 to 5.5 ms (~0 to 4.2 m) (Fig. 22 – U2). Unit 2 is generally thickest within the western portion of the study area where it fills available accommodation created by underlying stratigraphy (Figs. 5 – 7, 12, 14, 16, 17, 19, 20). This unit shallows toward the east and the valley margins (Figs. 8, 13, 19, 20), as well as over fluvial terraces (Figs. 9, 18, 19), where there is less accommodation is present. Erosion at the base of this unit along H3 is observed to truncate reflections within underlying seismic units U3 (Figs. 7, 8, 10, 11, 15, 19, 20) and U4 (Figs. 5, 14). The U-shaped channels which describe seismic facies SF2, and compose U2, are generally ~15 m wide and 0.75 ms (~0.5 m) deep (Figs. 6 – 8, 10 – 18). These are propagated upwards throughout the section, effectively preserving this channel-form throughout its cut-and-fill history. Cores through this unit indicate its composition varies from mostly muddy sediments (Fig. 16) to mud interbedded with numerous sand layers (Figs. 13 – 15, 17, 18).

These observations, along with high percentages of the benthic foraminiferal assemblage *Elphidium* (Standring et al., 2019), suggest Unit 2 formed in an outer bay environment- a high-energy environment just landward of the paleo-barriers subject to frequent variations in energy

source, ranging from tidal, storm, and wave processes (Dalrymple et al., 1992; Zaitlin et al., 1994). Radiocarbon dates within this unit suggest it began forming no later than ~8.5 ka, lasted until ~6.9 ka (Standring et al., 2019).

4.3.3 Unit 3 – Tidal Fill (U3)

U3 has an upper boundary of H2 and H3, and a lower boundary of H4/H4a/H4b (Figs. 5, 7 – 13, 15, 17, 19, 20). This unit is generally composed of SF4 and SF5 (Figs. 7, 8, 11, 15, 20), but occasionally displays SF1 near the bottom of the unit (Figs. 10, 11, 15), and SF2 and SF3 within the unit (Figs. 8, 10, 12, 13, 15, 17).

This unit ranges in thickness from ~0 to 16 ms (~0 to 12 m) (Fig. 22 – U3), and is thickest within the seaward portion of the study area where it infills an ~11 km long, 3.5 to 5 km wide channel-like feature along horizon H4/H4a that rapidly shallows landward and to the west (Figs. 5, 9, 19). The fill of this large channel-like feature is composed of SF4, but rapidly changes to SF3 in the landward portion of the study area (Figs. 12, 17).

Additionally, U3 is observed within the eastern portion of the study area overlying the erosive, channelized horizon H4/H4b, and composed of SF1 and SF5 (Figs. 8, 10, 11, 15, 20), but rapidly transitions to SF2 within the unit (Figs. 8, 10, 13, 15).

Based on this unit's stratigraphic position, the highly erosional and channelized nature of its basal horizons H4, H4a, and H4b, this unit is interpreted as tidal fill encompassing both tidal inlet and tidal delta sediments. This is a high tidal energy environment proximal to the barriers (Dalrymple et al., 1992; Zaitlin et al., 1994). Unit 3 is divided into two sub-units U3a and U3b based on their associated with SF4 and SF5, respectively.

4.3.4 Unit 3a – Tidal Inlet Fill (U3a)

U3a has an upper boundary of H3, and a lower boundary of H4a (Figs. 7, 12, 17, 20). This unit is composed of SF4 within the seaward portion of the study area (Figs. 7, 20), and SF3 within the landward portions of the study area (Figs. 12, 17). This unit varies in thickness from ~0 to 16 ms (~0 to 12 m) (Fig. 22 – U3a). U3a is thickest toward the seaward portion of the study area within an 11 km long, 1 to 2 km wide, 16 ms (~12 m) deep channel along horizon H4a that curves toward the northwest, interpreted as the tidal inlet (Fig. 22 – U3a). Although this unit is present within an 11 km long channelized feature, the highly erosive nature of its basal horizon H4a is most evident within the first 5 km of the seaward portion of the study area (Fig. 21 – H4a). Within this erosive channel-form, U3a is composed of SF4, characterized by internal reflections that onlap adjacent erosional surfaces within the unit, and are generally arranged in a draping pattern that reflects its deeply incised, channelized lower boundary. This cut-and-fill reflector configuration is indicative of multiple aggradational packages separated by periods of erosive channel formation, which is commonly observed within paleo-tidal inlets (Siringan and Anderson, 1993; Anderson et al., 2008; Storms et al., 2008; Ronchi et al., 2018, 2019). U3a transitions to SF3 toward the landward portion of the study area, consisting of low-amplitude, parallel, laminated to transparent reflections (Figs. 12, 17). Coring through the landward portion of this unit reveals it is mostly composed of mud with some sandy intervals containing foraminiferal assemblages indicative of a central bay environment (Fig. 17). A radiocarbon date found within PC-2 returns a date of ~8.5 ka for this unit (Fig. 17; Standring et al., 2019). The landward transition in seismic facies from draping, onlapping reflections (SF4) to parallel, laminated reflections (SF3) filling the tidal inlet has been interpreted as the stratigraphic

response to filling an empty tidal inlet, resulting in SF4, versus filling an almost-completely filled one (e.g., Storms et al., 2008; Zecchin et al., 2008; Ronchi et al., 2018, 2019).

4.3.5 Unit 3b – Tidal Delta Fill (U3b)

U3b has an upper boundary of H2 and a lower boundary of H4b (Figs. 8, 10, 11, 13, 15, 20). This unit is generally composed of SF1 and SF5 near its base (Figs. 8, 10, 11, 15, 20), and SF2 within the unit (Figs. 8, 10, 13, 15). U3b ranges in thickness from ~0 to 9 ms (~0 to 7 m) (Fig. 22 – U3b), where it is thickest within 11 km long, 50 to 75 m wide, 5.5 to 9 ms (~4 to 7 m) deep channels that meander along the eastern portion of the study area, and thinnest along the valley margins (Fig. 22 – U3b). SF5 is common within the base of these channels: unidirectional dipping internal reflections that display progradation and lateral accretion (Figs. 8, 11, 15, 20). Seismic characteristics of this nature have been commonly associated with tidal deltas (Siringan and Anderson, 1993; Rodriguez et al., 1998, 2005; Anderson et al., 2008). SF1 is also common within the base of these channels, observed as chaotic to discontinuous reflections with internal truncations (Figs. 10, 11, 15). Commonly, SF5 lies adjacent to SF1 (Figs. 11, 15), where unidirectional dipping reflections (SF5) transition into chaotic to discontinuous reflections (SF1) within a short distance. It is possible that stratigraphically these facies both represent dipping, laterally accreting strata composing the tidal delta unit, but is at times not well-imaged either due to large grain sizes or unfavorable dip directions, resulting in SF1.

Coring of this unit by GC-2 further lends support for the interpretation that U3b is a tidal delta (Fig. 15), in which its unidirectional dipping, laterally accreting reflections are observed to be composed of muds with numerous layers of silty sand. Carbon dates taken from the transition

from tidal delta to outer bay sediments in GC-2 (Fig. 15) provided ages of ~8.5 ka, confirming this tidal delta was active during this time (Standring et al., 2019).

SF2 is also common within this unit: a facies composed of high-amplitude, U-shaped, aggrading reflections commonly associated with an outer bay environment proximal to the barriers (Figs. 8, 10, 13, 15). This marked change from laterally accreting to aggrading reflections is likely due to a change in tidal regime associated with the infilling of the tidal inlet by ~8.5 ka, as observed in PC-2 (Fig. 17). Thus, as the tidal inlet unit U3a infilled by ~8.5 ka, the adjacent tidal delta unit U3b reflected this change in tidal regime by switching from a laterally accreting (SF1/SF5) to an aggrading (SF2) seismic facies.

4.3.6 Unit 4 – Central Bay (U4)

U4 has an upper boundary of H2, H3, and H4, and a lower boundary of H5 (Figs. 5 – 10, 12 – 20). This unit is primarily composed of SF3 (Fig. 6 – 8, 12 – 18, 20). U4 varies in thickness from ~0 to 11 ms (~0 to 8.5 m) (Fig. 22 – U4). This unit is generally thickest within the western portion of the study area, passively filling accommodation left by underlying stratigraphy, and thinnest along the eastern margin where tidal-related horizons H4, H4a and H4b have heavily reworked it (Figs. 5, 7 – 10, 15, 19, 20).

Coring of this unit indicates U4 is composed of mostly fine-grained mud, with some interbedded muddy sand intervals (Figs. 14, 16 – 18). This fine-grained composition, along with foraminiferal evidence of a spike in *Ammonia* (Strandring et al., in prep), support the interpretation that these sediments were deposited in a low-energy, quiescent central bay environment landward of the barriers (e.g., Dalrymple et al., 1992; Zaitlin et al., 1994; Rodriguez et al., 2005; Anderson et al., 2008). Carbon dates from this unit indicate that this environment

initiated as early as ~9.6 ka (Fig. 17) and lasted until ~8.0 ka, when it transitioned to an outer bay environment (Fig. 17, 18; Standring et al., 2019).

Although U4 is generally thickest in the western portion of the study area, U4 reaches it maximum thickness in the form of three mound-like features measuring ~500 m in width, ~8 m in height (Figs. 5, 7, 9, 19, 20, 22). Goff et al. (2016) have interpreted similar mound-like features in Corpus Christi Bay, Texas as oyster reefs, described as having a high-amplitude, draping reflection as its upper boundary, a chaotic to acoustically blank interior, a varying amplitude, planar reflection at its base, and adjacent onlapping reflections. A similar configuration is observed within the mound-like features in this study, having a high-amplitude upper boundary defined by H4, H4a, and H4b, a chaotic to acoustically blank interior associated with SF3, a varying amplitude lower boundary defined by H5, and adjacent onlapping reflections by U3a and U3b (Fig. 7, 20). Unfortunately, these mound-like features were not groundtruthed, and their depositional environment cannot be confirmed without further investigation.

4.3.7 Unit 5 – Bayhead Delta (U5)

U4 has an upper boundary of H2, H4, and H5 and a lower boundary of H6 (Figs. 5 – 20), and varies in thickness between ~0 to 23 ms (~0 to 17.5 m) (Fig. 22 – U5). This is the thickest unit observed in this study, composing over half of the total incised valley fill. This unit is thinnest along the flanks of the valley (Fig. 5, 6, 8, 16, 20), above or adjacent to underlying Pleistocene fluvial terraces (Fig. 9, 17 – 19), or when it is heavily reworked by tidal-related horizons units H4, H4a, and H4b within the seaward portion of the study area (Figs. 7, 8, 11, 15, 19, 20). U5 is thickest when it is filling in accommodation provided by the underlying fluvial geology (Figs. 5, 9, 12, 19). This is clearly observed as the topography of its lower bounding

horizon H6 (Fig. 21 – H6) correlates well with the lateral variations thickness observed in U5 (Fig. 22 – U5).

This unit is primarily composed of high-amplitude, laterally accreting to aggrading reflections (Figs. 5 – 18; Swartz, 2019; Thomas, 1991). Coring of this unit reveals it is composed of very fine to fine sands, organic rich muds and clays, and clays interbedded with find sandy layers with organic wood fragments and plant debris (Fig. 12, 17, 18; Thomas, 1991). Lack of foraminifera in these sediments suggest a terrestrial depositional environment. Therefore, sediments in U5 are interpreted as deriving from an upper bay or bayhead delta environment (Swartz, 2019).

Age models from cores PC-2 (Fig. 17) and PC-4 (Fig. 18) indicate that the environment transitioned from fluvial to upper bay ~9.8 ka (Standring et al., 2019). This upper bay environment lasted until at least ~8.8 ka as the system was inundated and transitioned into a central bay environment (Fig. 18).
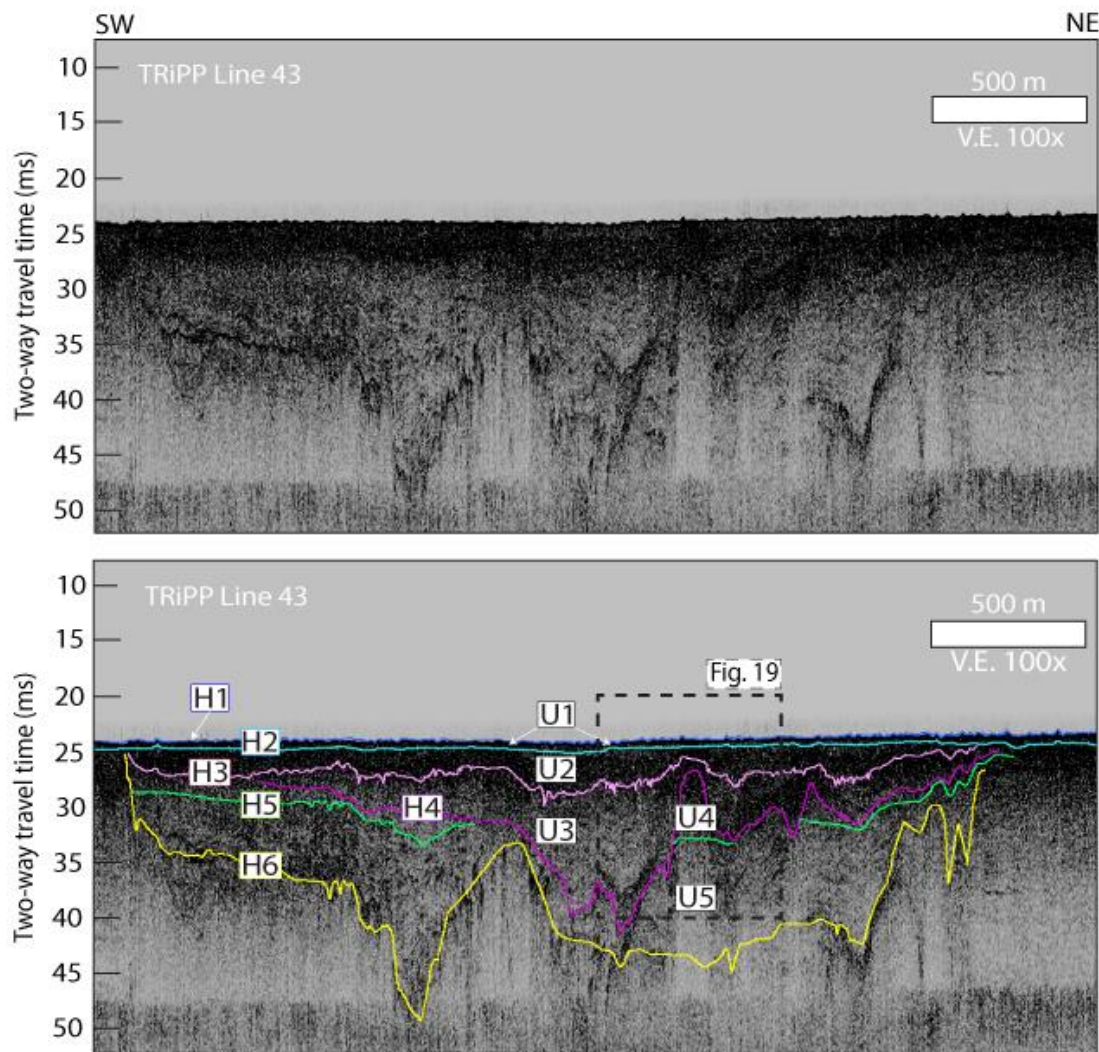
Figure 19: Uninterpreted (top) and interpreted (bottom) envelope chirp data of strike-oriented Tripp Line 43 displaying the seismic horizons (H1-H6) that bound seismic units (U1-U5) within this study. This is the seaward-most strike-oriented line in this study, displaying a very narrow incised valley extent (~2.5 km in width) funneling the tidal inlet and delta (U3) toward the eastern (right) side of the valley. Inset indicates the locations for Figure 21. The location for this chirp line can be found in Figure 3.
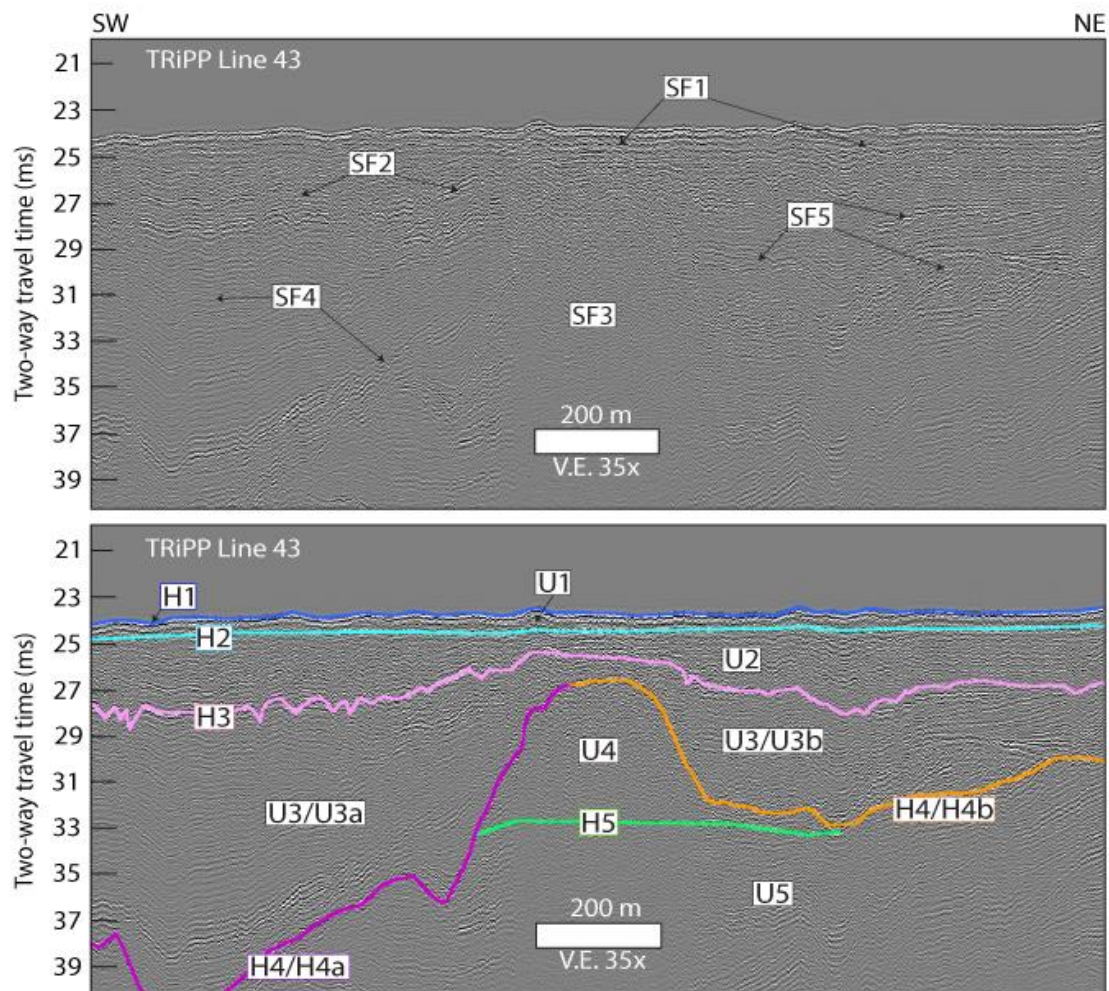
Figure 20: Top – Seismic facies analysis of full-waveform data on Tripp Line 43. Bottom – Interpretation of full-waveform data on Tripp Line 43. Displayed here is a strike-oriented line, highlighting the differences in seismic facies composing U3/U3a (SF4 = tidal inlet) and U3/U3b (SF5 = tidal delta). Both of these units' lower-bounding horizons (H4/H4a and H4/H4b) truncate H5. H3, which forms the lower boundary of U2, is observed to truncate reflections composing U3/U3a-b. U2 is composed of SF2, characterized as U-shaped, aggrading reflections, which are subsequently truncated by H2. H1 is the seafloor. The location for this chirp line can be found on Figures 21 and 3.

Figure 21: Time-structure maps, measured in milliseconds two-way travel-time, of seismic horizons mapped in this study. When relevant, these values are converted to depth (mbsl) using an average velocity of 1525 m/s (Abdulah et al., 2004).

Figure 22: Time-thickness maps, measured in milliseconds two-way travel-time, of seismic units mapped in this study. When relevant, these values are converted to depth (mbsl) using an average velocity of 1525 m/s (Abdulah et al., 2004).
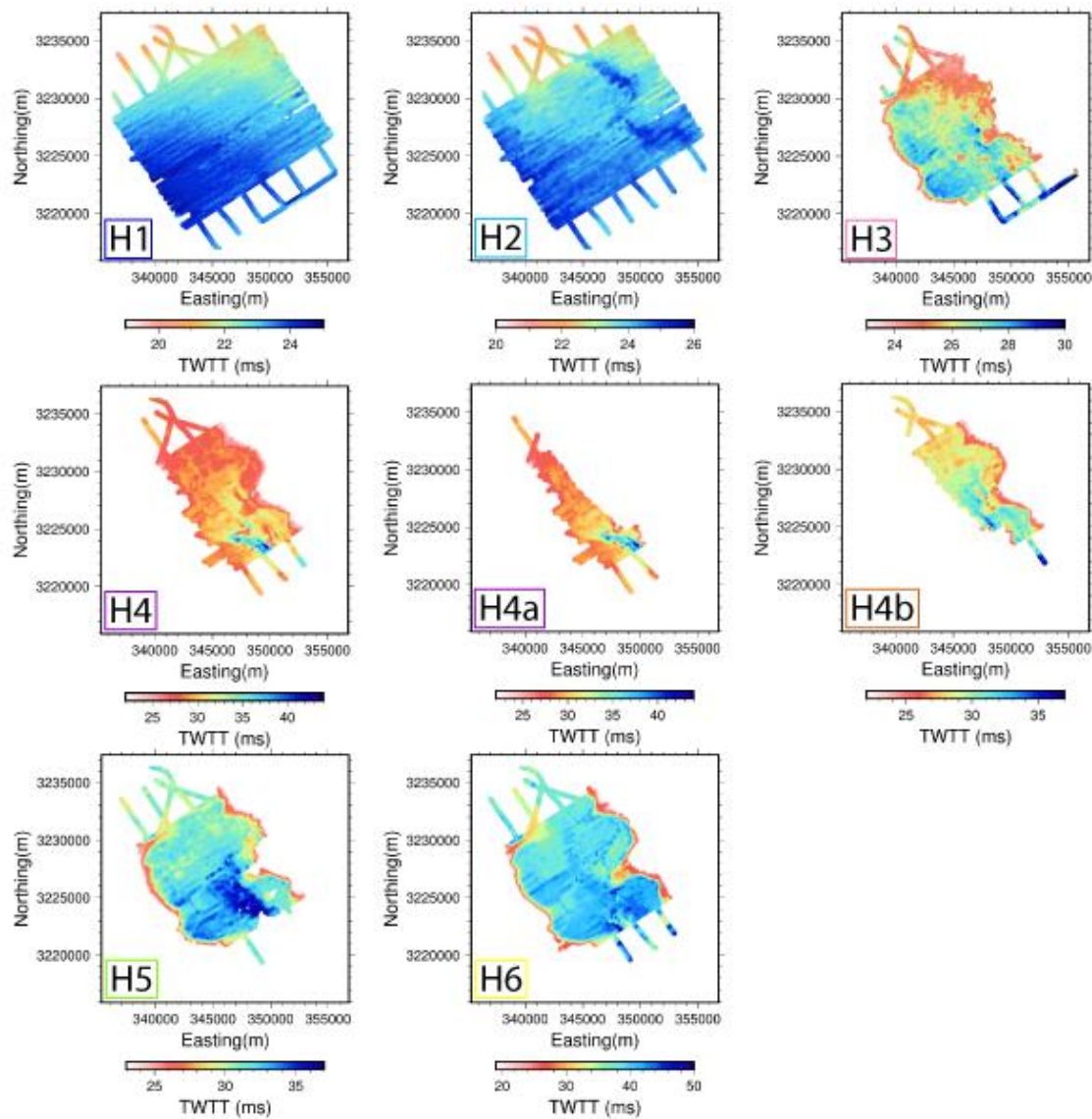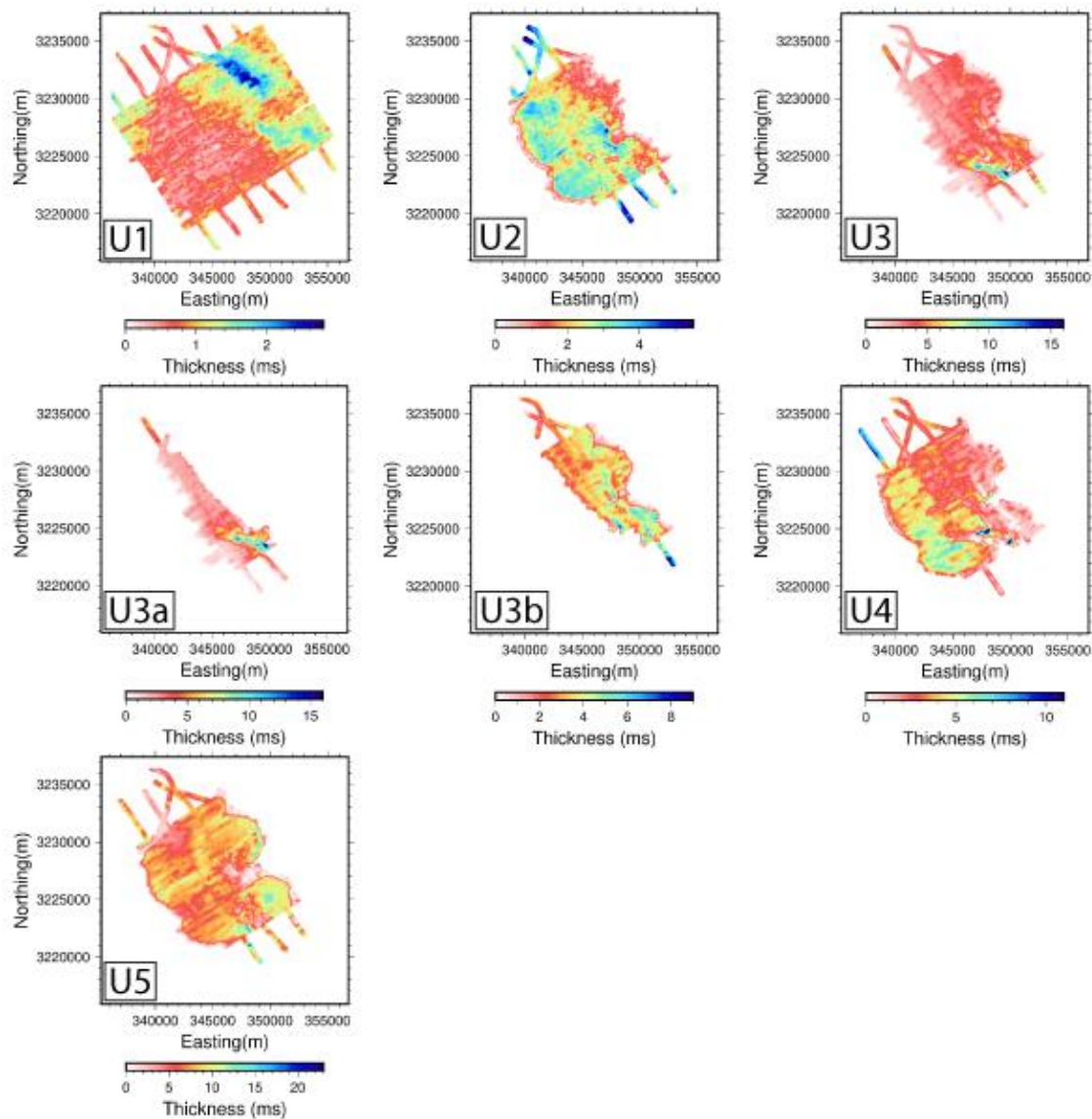
5. Discussion

5.1 Preservation of Estuarine Deposits

As rising sea levels act upon a barrier island system, features of the coastal lithosome are generally eroded by wave, storms, and tidal forces associated with the transgressive ravinement (e.g., Swift and Thorn, 1991; Cattaneo and Steel, 2003). Commonly referred to as a "wave ravinement surface" (e.g., Allen and Posamentier, 1993; Cattaneo and Steel, 2003) to highlight the erosive mechanism, the creation of this surface has also been attributed to downwelling coastal storm currents (Swift and Thorn, 1991) and major storms (Goff et al., 2015). Generally, this strong erosive action removes estuarine sediments, and transfers eroded sediment seaward from the barrier island system to the marine sediment sheet overlying the ravinement. Due to the erosive nature of the transgressive ravinement, subaerial and shallow features of the barrier island system, including the barriers themselves, are often removed, preserving only deep back-barrier sediments, such as bay and tidal facies, within the stratigraphic record (Ronchi et al., 2018; Ronchi et al., 2019).

There have been documented studies within the Adriatic Sea (Storms et al., 2008) and Tijucas Bay, Brazil (Cooper et al., 2016), investigating the preservation of the barriers throughout transgression through a process called "overstepping", in which the barrier is stranded on the continental shelf as a marine sand body (Carter, 1988). The overstepping and preservation of the barrier during transgression has been attributed to rapid sea-level rise, rapid increase in back-barrier accommodation, little wave action, or rapid burial by shoreface sediments (Storms et al., 2008; Cooper et al., 2016).

This is one interpretation of paleoshoreline evolution across the northern Gulf of Mexico, wherein Sabine and Heald Banks are interpreted as relict, overstepped barriers preserved on the inner shelf as sand bodies (Fig. 2; Rodriguez et al., 1999; Rodriguez et al., 2004). Sabine bank is located approximately 30 km offshore in water depths of 5 to 12 m, while Heald banks is

approximately 45 km offshore in 9 to 15 m water depth. Rodriguez et al., 2004 claim that these shorelines retreated over terraced fluvial deposits within the Trinity-Sabine incised valley, which served as local sand sources for barrier island stabilization and persistence throughout sea-level rise. These barriers were then overstepped and stranded on the inner shelf as isolated sand bodies once these fluvial sand sources were depleted, sea-level rise reached a critical threshold, or both (Rodriguez et al., 2004).

Conversely, it has been proposed that the origin of modern sand banks is not as drowned, overstepped, detached barriers (i.e., Snedden et al., 1999), but rather as modern marine deposits that have reworked underlying remnant estuarine and tidal deposits (Thomas and Anderson, 1994; Dyer and Huntley, 1999). Thomas and Anderson (1994) observe that Sabine and Heald Banks overlie a ravinement reworking underlying estuarine and tidal delta facies. Thus, it is possible that these sand banks have a marine origin, which have formed from the reworking of remnant estuarine and tidal facies, rather than as downed, overstepped barriers.

In this study, erosion associated with the transgressive ravinement, interpreted as the H2 horizon, has significantly reworked underlying estuarine sediments (Figs. 5 – 20), and completely eroded and removed the barrier within our study area. Observations of interpreted overstepped barriers include elongated, shore-parallel sand bodies with reflectors that prograde both seaward and landward, with a coarsening-upward stratigraphic composition (Storms et al., 2008; Cooper et al., 2016). These seismic stratigraphic and lithologic indicators are not observed within this study, supporting the interpretation that the paleo-barrier within this study area was not overstepped, but instead completely removed by transgressive erosion.

Despite significant transgressive erosion, considerable preservation of deltaic (U5) and back-barrier (U2 – U4) strata is observed in this study (Figs. 5 – 20). The transgressive

ravinement (H2) is observed to rework shallow back-barrier units (U2, U3, U3a, U3b), while only reworking the distal flanks of the deeper central bay and bayhead delta units along the valley edges (U4, U5). Although preservation of the barrier can give excellent insights into the mode in which the estuarine system transgressed (i.e., erosional, rollover, overstepping – Carter, 1988), preserved deltaic, bay, and tidal facies can provide convincing spatial and temporal evidence for understanding the morphological evolution of the estuarine system throughout transgression (i.e., Ronchi et al., 2018; 2019).

5.2 Estuarine Interaction with Underlying Geology

Heterogeneity in the underlying, antecedent geology in which the barrier island system transgresses has long been recognized as a major control on its evolution (e.g., Belknap and Kraft, 1985; Riggs et al., 1995, Mallinson et al., 2018; Shawler et al., 2020). These are often paleodrainage systems that cut into the landscape by fluvial incision during subaerial exposure, and now filled with fluvial, coastal, and shelf facies as the system was flooded (e.g., Allen and Posamentier, 1993; Dalrymple et al., 1992; Zaitlin et al., 1994). Deep, topographic lows cut by the paleodrainage system form the incised valley and are important in defining the estuaries which transgress them, including controlling the location of the tidal inlet (Morton and Donaldson, 1973). Additionally, topographic highs in the form of fluvial interfluves and terraces provide both increased elevation in which barrier islands are pinned upon (e.g., Raff et al., 2018; Shawler et al., 2020), as well as sediment supply to the barrier via wave and tidal forces (e.g., Riggs et al., 1995; Anderson et al., 2016; Hollis et al., 2019). This study supports this growing body of literature, and finds that the estuarine system is intimately controlled by its antecedent geology.

The underlying fluvial topography, interpreted as horizon H6 (Figs. 21, 23B-C), is observed to control the morphology of all overlying units by providing accommodation in which subsequent stratigraphic units fill. H6 is observed as a channelized, erosional surface within the seaward portion of the study area, reaching depths of ~50 ms (~38 mbsl), and that gradually shallows landward within the valley to ~22 ms depth (~29 mbsl) (Figs. 21, 23B-C). Where H6 is relatively deep, accommodation is created in which overlying units preferentially fill. This is clearly observed as the deep topography of H6 along the eastern and western flanks of the seaward portion of the study area correlate well with the lateral variations in thickness of seismic units U5, U4, U3, U3a, U3b and U2 (Figs. 21, 22). This is compounded by the observation that channels created by the underlying fluvial surface are propagated upward throughout the stratigraphic section, owing to the influence in which this surface has on the spatial variations in channelization of strata above (Figs. 5, 9, 11, 18, 19).

Beyond creating accommodation for estuarine sediments to fill, the morphology of the incised valley itself appears to promote barrier island initiation. Figure 23A displays a 20 ms envelope median coherency extracted for the approximate base of the Trinity incised valley (Swartz, 2019). This coherency extraction, although likely incorporating anomalous amplitudes throughout the entire incised valley fill, shows the presence of sinuous channel forms, shallow fluvial terraces, lateral accretion surfaces, and a well-defined overall valley extent (Swartz, 2019). In the seaward-most portion of the study area, the valley extent narrows to ~2.5 km in width (Fig. 21, 23A), which rapidly widens landward to ~10 km in width (Fig. 5, 23A) over a distance of ~1 km (Fig. 23A). This framework effectively "bottlenecks" the estuarine system, promoting tidal units (U3, U3a, U3b) to preferentially deposit along the seaward and eastern portions of the study area (Figs. 19, 22, 23D). The influence of the valley extent on determining

the location of tidal deposits, and by proxy paleo-barrier island position (e.g., Thomas and Anderson, 1994; Rodriguez et al., 2004; Anderson et al., 2016), is best seen in Figure 11, where reflectors associated with the tidal delta unit (U3b) switch dip direction from landward-dipping to seaward dipping. Dip direction is a key indicator of flow direction, interpreted as landward-dipping, flood-tidal delta deposits, and seaward-dipping, ebb-tidal delta deposits (e.g., Rodriguez et al., 1998; Anderson et al., 2008). The presence of a fluvial terrace underlying this switch in tidal flow direction is thus interpreted as the underlying fluvial topography providing a direct "pinning point" for the barrier (e.g., Raff et al., 2018; Shawler et al., 2020). However, the underlying fluvial geology does not act as a sediment source for the paleo-barrier island system, which may be expected from previous studies (e.g., Riggs et al., 1995; Anderson et al., 2016; Hollis et al., 2019; Shawler et al., 2020). This is demonstrated by the top of fluvial sediments (H6) very rarely being truncated and reworked by overlying tidal (H4, H4a, H4b) or wave erosional surfaces (H2) (Figs. 5, 7 – 9, 11, 19). Instead, sediment sources reworked by tidal units U3, U3a, and U3b, and supplied to the barrier island system, are preferentially from the bayhead delta (U5) and central bay (U4) units (Figs. 5, 7 – 10, 15, 19, 20).

In addition, the relatively shallow fluvial topography within the landward portion of the study area provides decreased accommodation within the back-barrier, promoting the aggradation of barrier-proximal outer bay unit (U2) for ~2.5 ka (Figs. 5 – 20; Standring et al., 2019). The transition from an active tidal inlet and tidal delta to an outer bay environment occurred ~8.5 ka (Figs. 17, 18; Standring et al., 2019), indicating the deactivation and infilling of the tidal inlet at this point. This evolution is manifested by the lower bounding surface of the outer bay unit (H3) truncating strata within tidal units, and depositing channelized, aggradational outer bay strata above (Figs. 7, 8, 10, 11, 15, 19, 20) until the onset of inner shelf sediments (U1)

~6.9 ka (Standring et al., 2019). The deactivation of a tidal inlet has been proposed to be followed by the complete overstepping and in-place drowning of the barrier island system, wherein an abrupt increase in back-barrier accommodation would increase tidal prism, drown low-lying marshes and tidal flats, and lead to the complete drowning of the estuary (FitzGerald et al., 2006; Fitzgerald et al., 2008; Storms et al., 2008; Ronchi et al., 2019). However, following the deactivation and closure of the tidal inlet, the landward increasing fluvial elevation helped to promote the vertical aggradation of outer bay strata, and possibly stability for the barrier island system, as opposed to retrogradation and barrier disintegration or overstepping associated with an increase in back-barrier accommodation. This finding therefore agrees with previous studies suggesting the reduced back-barrier accommodation provided by antecedent topographic highs can stabilize a barrier island system (e.g., Shawler et al., 2020).
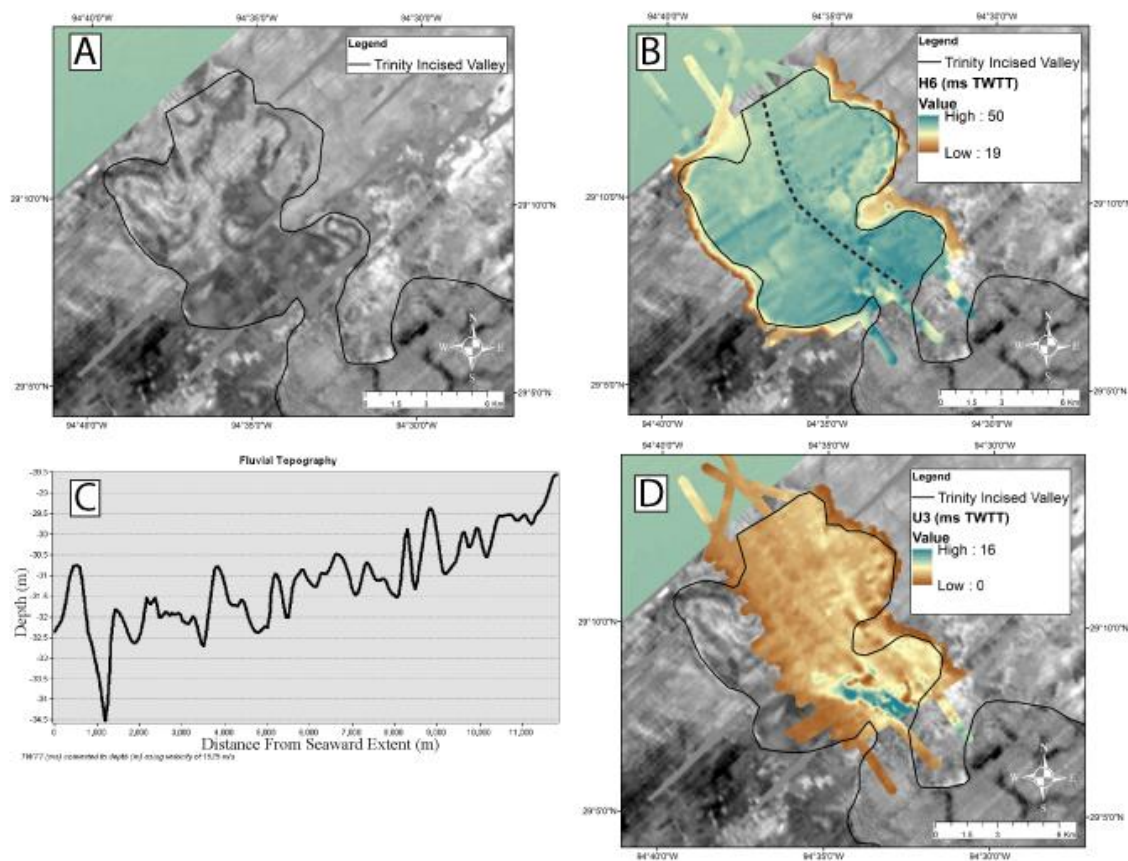
Figure 23: A) Coherency attribute extracted from 3D seismic data (modified from Swartz, 2019). Extraction displays sinuous channel forms, shallow fluvial terraces, lateral accretion surfaces, and a well-defined overall valley extent (bold black polygon). Valley observed to "bottleneck" toward the seaward extent, increasing from ~2.5 km in width, to ~10 km in width over a distance of ~1km. B) A time-structure map of horizon H6, which is interpreted to be the top of fluvial strata, overlays the 3D coherency extraction. A topographic profile track is shown as a dotted line traveling up-dip. C) A topographic profile graph from panel B. Profile is taken over a depth-converted structure map of H6 to reflect the landward increase in elevation of the underlying, antecedent fluvial geology. D) A time-thickness map of U3, interpreted as the thickness of tidal deposits in the study area. Maximum thickness is seen within the tidal inlet, displayed as an ~5 km long, 1 to 2 km wide, 16 ms (~12 m) deep channel. The extremely narrow extent of the incised valley is interpreted to control the preferential deposition of tidal inlet and tidal delta deposits along the seaward and eastern portions of the valley.

5.3 Paleo-barrier Island Evolution

The initiation of the estuarine system within this study area is proposed to occur ~9.8-9.6 ka (Figs. 24-B), indicated by the transition from a fluvial to upper bay/bayhead delta environment in cores PC-2 (Fig. 17) and PC-4 (Fig. 18; Standring et al., 2019). During this time, it has been proposed that a large, 75 km long estuary extended from approximately 20 km offshore modern Galveston Bay, to seaward of Thomas Bank (Fig. 24A; Thomas and Anderson, 1994; Anderson et al., 2008, 2016). Thomas and Anderson (1994) identified a paired tidal inlet and upper bay/bayhead delta facies bound by upper and lower flooding surfaces, in which the tidal inlet facies was located just seaward of Thomas Bank (Fig. 24A). A flood tidal delta facies was identified extending landward ~20 km from this tidal inlet location. The upper bay/bayhead delta sequence was located depositing within and landward of the confluence of the Trinity-Sabine river valleys, and of which its most landward extent reached into this study's area of focus (Fig. 24A). Dating of this parasequence shows it initiated by ~10 ka (Thomas and

Anderson, 1994), agreeing well with dates within cores PC-2 (Fig. 17) and PC-4 (Fig. 18) that an upper bay/bayhead delta environment existed within this study's area of focus during this time. Thus, we suggest that the upper bay/bayhead delta deposits observed in this study, identified as seismic unit U5, initiated ~9.8 – 9.6 ka, and represents the landward-most component of an estuary extending almost 75 km seaward (Figs. 24A-B; Thomas and Anderson, 1994).

At approximately 8.8 ka, the area transitioned from an upper bay/bayhead delta environment to a central bay environment (Figs. 24C-D), although PC-2 provides a date within this unit of ~9.6 ka (Figs. 17, 18; Standring et al., 2019). The deposition of central bay sediments (U4) draped on top of bayhead delta strata, passively filling accommodation, but was largely confined within the valley walls (Figs. 5, 6, 8, 16, 19, 24C-D). Although the true extent of the bay may have extended beyond the valley extent, severe subsequent reworking by the tidal (H4, H4a, H4b) (Figs. 5, 7 – 10 , 15, 19, 20) and transgressive (H2) ravinements (Fig. 8, 16) limits this interpretation. It is also likely that the initiation of the tidal inlet and delta (U3a, U3b) occurred during this time (Figs. 24C-D), as carbon dates provided in GC-2 (Fig. 15) and PC-2 (Fig. 17) provide an age of at least 8.5 ka (Standring et al., 2019). The extreme narrowing of the incised valley within the seaward and eastern portion study area effectively controlled the spatial extent of the tidal inlet and delta, and thus the location of barrier island (Fig. 23D, 24C-D).

These data are inconsistent with previous interpretations which assert a barrier island existed adjacent to Shepard and Heald Banks from 8.7 to 7.7 ka (Thomas and Anderson, 1994; Rodriguez et al., 2004). Thomas and Anderson (1994) observe a large tidal delta deposit within the Trinity-Sabine valley extending seaward from Heald Bank to just landward of Thomas Bank (Fig. 24C). However, this tidally influenced facies lacks evidence of a tidal inlet deposit, which can be more precise in locating paleo-barrier position than solely tidal deltas due their smaller

and more discrete geographic extent (e.g., Thomas and Anderson, 1994). Additionally, Rodriguez et al., (2004) interprets estuarine strata beneath Heald Bank with dates ranging from 8.4 to 7.7 ka. They describe this facies as consisting of landward-dipping seismic reflectors, characteristic of a flood-tidal delta's landward transport direction, and indicates the paleoshoreline lies seaward of this location. However, the seismic data in which these cores were tied to were of low quality (Rodriguez et al., 1999), and the direction of dipping reflectors may be untrustworthy without reprocessed and/or new geophysical data. Therefore, this large tidal delta deposit, given its age constraints of 8.7 to 7.7 ka, possibly represents the ebb-tidal delta component of the barrier island system initiating ~8.8 ka within this study's area of focus (Fig. 24C). However, sparse geophysical data between these two areas hinder conclusive evidence for how this tidal facies relates to this study.

By ~8.5 ka, the estuarine system experienced a major shift from central bay (Fig. 17, 18) and tidal inlet and delta environments (Figs. 13, 17), to that of an outer bay environment (Figs. 24E-F; Standring et al., 2019). This is a high-energy environment just landward of the barrier inclined to a mixture of tidal, storm, and wave processes (Dalrymple et al., 1992; Zaitlin et al., 1994). This led to the closure and infilling of the tidal inlet and tidal delta units, providing a total lifespan of the tidal system of ~300 years (Figs. 24E-F). Rather than a complete overstepping and in place drowning of the estuary, which is expected following the deactivation of the tidal inlet (e.g., FitzGerald et al., 2006, FitzGerald et al., 2008), reduced back-barrier accommodation provided by increased landward antecedent topography (Figs. 23B-C, 24E-F) helped to promote the aggradation of outer bay sediments, and barrier island stability for the next ~1.6 kyr.

By ~6.9 ka, cores GC-2 and GC-5 indicate a shift to an inner shelf environment, leading to the deposition of U1 (Figs. 14, 15, 24G-H; Standring et al,. 2019). During this time, the paleo-

barrier retreated and degraded, as evidenced by multiple washover deposits overlying an erosive transgressive lag in GC-6 (Fig. 13). This barrier-related material filled multiple 2 to 4.5 km long, 1.3 to 1.5 km wide, 0.75 to 2.8 ms (~1 to 2 m) deep channel-like features focused on the eastern side of the valley (Fig. 22 – U1, 24G-H). It is possible that the preservation of this unit is focused on the eastern side of the valley (Figs. 24G-H) due to its heavy reworking of underlying mud-rich outer bay and sand-rich tidal delta units (Figs. 5, 8, 13), as opposed to the western side of the valley where it predominantly reworks solely mud-rich outer bay and central bay units (Figs. 5, 6, 8, 16). Barrier retreat and degradation along the eastern side of the valley persisted until at least ~4.3 ka, as observed by a dated transgressive lag shell in GC-6 (Fig. 13), while the western side of the valley rapidly transitioned into an inner shelf environment. During this ~1.7 kyr span, the estuarine system was likely inundated by marine sediments, the barrier was degrading, and the shoreline was landward of the study area, possibly forming the Galveston Island by 5.3 ka and Bolivar Peninsula by 2.8 ka (Fig. 24G; Rodriguez et al., 2004; Standring et al., 2019); however, the lack of data between this study's focus area and the modern shorelines hinder the ability to analyze the paleoshoreline evolution past ~6.9 ka as observed in cores GC-2 (Fig. 15) and GC-5 (Fig. 16).
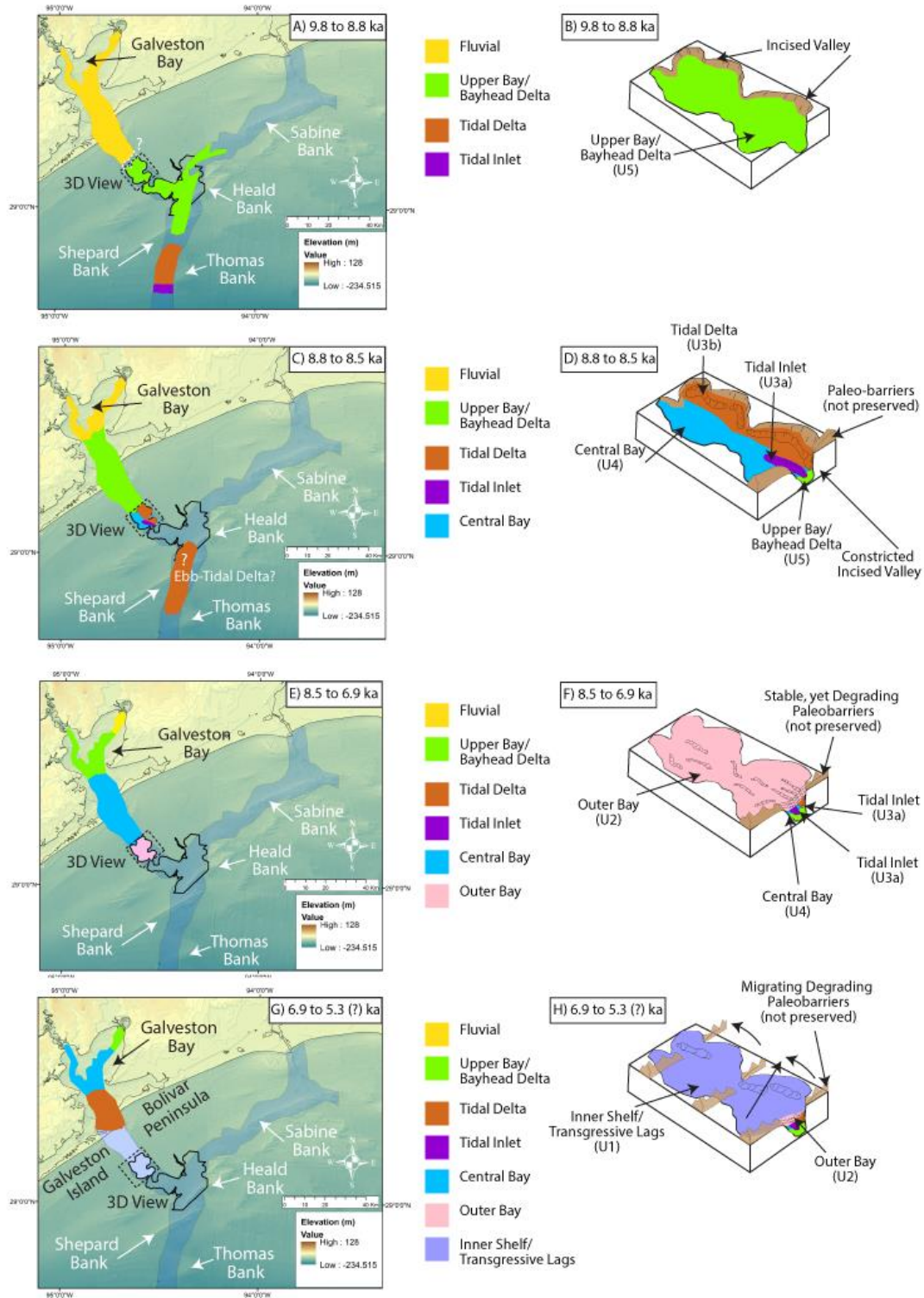
Figure 24: A) Paleoshoreline evolution map from 9.6 to 8.8 ka for the northern Gulf of Mexico inner shelf. The Trinity-Sabine incised valley is drawn as an opaque blue polygon, and is from Thomas and Anderson (1994). A revised interpretation of the Trinity incised valley from Swartz (2019) is displayed as a bold dark polygon.

Locations and extent for tidal inlet, tidal delta, and upper bay/bayhead delta are modified from Thomas and Anderson (1994). Fluvial extent is modified from Anderson et al. (2008), although the boundary between fluvial and upper bay/bayhead delta facies is not available, as denoted by a white question mark and dotted boundary. Black dotted box represents outline of 3D schematic in the following figure. B) Three-dimensional schematic of the portion of the Trinity incised valley within this study's area of focus. An upper bay/bayhead delta facies, identified in this study as seismic unit U5, deposits within the valley overlaying fluvial sediments. C). Paleoshoreline evolution map from 8.8 to 8.5 ka for the northern Gulf of Mexico inner shelf. The fluvial and bayhead delta locations and extent are modified from Anderson et al. (2008). Facies within the dotted black box (tidal inlet, tidal delta, central bay) are mapped and interpreted within this study. The tidal delta facies lying ~30 km seaward, and adjacent to Heald and Sabine Banks, has been modified from Thomas and Anderson (1994). This has been re-interpreted as a possible ebb-tidal delta. D) Three-dimensional schematic of the Trinity incised valley within this study's area of focus. The estuarine system is initiated, and controlled by the underlying incised valley's constricted geometry. This results in the development of stable barriers, the deposition of central bay sediments (U4), and preferential deposition of tidal inlet (U3a) and tidal delta (U3b) deposits along the eastern portion of the valley. E) Paleoshoreline evolution map from 8.5 to 6.9 ka for the northern Gulf of Mexico inner shelf. Locations and extent for fluvial, upper bay/bayhead delta, and central bay deposits are from Anderson et al. (2008). F) Three-dimensional schematic of the Trinity incised valley within this study's area of focus. Stable, yet degrading barriers led to the closure of the tidal inlet (U3a) and tidal delta (U3b) units, and the widespread deposition of outer bay (U2) sediments. Decreased back-barrier accommodation space resulting from increased fluvial topography promoted aggradation and resilience of outer bay sediments as opposed to retrogradation and marine incursion. G) Paleoshoreline evolution map from 6.9 to 5.3 ka for the northern Gulf of Mexico inner shelf. Location and extent of upper bay/bayhead delta, central bay, and tidal facies are from Anderson et al. (2008). H) Three-dimensional schematic of the Trinity incised valley within this study's area of focus. Degrading barriers migrated landward across the study area, leading to the deposition of inner shelf/transgressive lag deposits (U1). Large channels composed of washover deposits and transgressive lags are remnants of the now-eroded barriers. The paleoshoreline at this time likely transgressed to Galveston Island by 5.3 ka (Rodriguez et al., 2004).

6. Conclusions

To investigate the role of antecedent topography in the evolution of an ancient barrier island system, we focus on the Trinity incised valley offshore modern Galveston Bay in the central Gulf of Mexico. We show that the underlying fluvial topography in which the barrier island system is transgressing plays a significant role in barrier island initiation and stability. Although there is little to no tidal reworking and redistribution of the underlying fluvial sediments, this section provides higher elevation and reduced accommodation for back-barrier sediments. This increased fluvial elevation promotes vertical aggradation of back-barrier sediments and barrier island stability as opposed to transgression and barrier island disintegration. Additionally, this study provides a methodology to study the evolution of a paleo-barrier island system with sparse preservation of the barrier itself; instead, we investigate preserved back-barrier (deltaic, bay, and washover) and tidal (tidal inlet, tidal deltas) sediments to construct the depositional and erosional evolution of this paleo-barrier island system. Lastly, we revise the established Holocene paleoshoreline model proposed by Rodriguez et al., 2004 to suggest that the model includes a paleoshoreline position within our study are landward of Heald Bank, in agreement with previous authors (Thomas and Anderson 1994; Anderson et al., 2016).

7. References

Abdulah, K.C., Anderson, J.B., Snow, J.N., Holdford-Jack, L., 2004. The late Quaternary Brazos and Colorado Deltas, Offshore Texas, U.S.A. — their evolution and the factors that controlled their deposition. In: Anderson, J.B., Fillon, R.H. (Eds.), Late Quaternary Stratigraphic Evolution of the Northern Gulf of Mexico Margin. Society for Sedimentary Geology, Special Publication 79, pp. 237–270.

Anderson, J.B., Abdulah, K., Sarzalejo, S., Siringan, F., Thomas, M.A., 1996. Late Quaternary sedimentation and high-resolution sequence stratigraphy of the east Texas shelf. Geol. Soc. Spec. Publ. 117, 95–124.

Anderson, J.B., Rodriguez, A., Abdulah, K.C., Fillon, R.H., Banfield, L.A., McKeown, H.A.,Wellner, J.S., 2004. Late Quaternary stratigraphic evolution of the northern Gulf of Mexico: a synthesis. In: Anderson, J.B., Fillon, R.H. (Eds.), Late Quaternary Stratigraphic Evolution of the Northern Gulf of Mexico Margin. Society for Sedimentary Geology, Special Publication 79, pp. 1–23.

Anderson, J.B., Rodriguez, A.B., Milliken, K., and Taviani, M., 2008, The Holocene evolution of the Galveston estuary complex, Texas: Evidence for rapid change in estuarine environments, in Anderson, J.B., and Rodriguez, A.B., eds., Response of Upper Gulf Coast Estuaries to Holocene Climate Change and Sea-Level Rise: Geological Society of America Special Paper 443, p. 89–104, doi: 10.1130/2008.2443(06).

Anderson, J.B.,Wallace, D.J., Simms, A.R., Rodriguez, A.B., Milliken, K.T., 2014. Variable response of coastal environments of the northwestern Gulf of Mexico to sea-level rise and climate change: implications for future change. Mar. Geol. 352, 348–366.

Anderson, J.B., Wallace, D.J., Simms, A.R., Rodriguez, A.B., Weight, R.W., and Taha, Z.P., 2016, Recycling sediments between source and sink during a eustatic cycle: Systems of late

Quaternary northwestern Gulf of Mexico Basin: Earth-Science Reviews, v. 153, p. 111–138, doi:10.1016/j.earscirev.2015.10.014.

Allen, G.P., Posamentier, H.W., 1993. Sequence stratigraphy and facies model of an incised valley fill: the Gironde estuary, France. Journal of Sedimentary Petrology 63, 378– 391.

Belknap, D.F., Kraft, J.C., 1981. Preservation potential of transgressive coastal lithosomes on the U.S. Atlantic shelf. Marine Geology 42, 429–442.

Belknap, D.F., Kraft, J.C., 1985. Influence of antecedent geology on stratigraphic preservation potential and evolution of Delaware's barrier systems. Marine Geology 63, 235– 262.

Carter, R.W.G., 1988. Coastal Environments: An Introduction to the Physical, Ecological and Cultural Systems of Coastlines. Academic Press, London.

Cattaneo, A., Steel, R.J., 2003. Transgressive deposits: a review of their variability. Earth Sci. Rev. 62, 187–228.

Cochrane, J.D., Kelly, F.J., 1986. Low-frequency circulation on the Texas–Louisiana continental shelf. J. Geophys. Res. 91, 10645–10659. http://dx.doi.org/10.1029/JC091iC09p10645

Cooper, J. A. ., Green, A. ., & Loureiro, C. (2018). Geological constraints on mesoscale coastal barrier behaviour. Global and Planetary Change, 168, 15–34. https://doi.org/10.1016/j.gloplacha.2018.06.006

Dalrymple, R.W., 1992. Tidal depositional systems. In: Walker, R.G., James, N.P. (Eds.), Facies Models—Response to Sea Level Change. Geological Association of Canada Publications, pp. 195–218.

Devine, P.E., 1991. Transgressive origin of channeled estuarine deposits in the Point Lookout Sandstone, Northwestern New Mexico: a model for Upper Cretaceous, cyclic regressive parasequences of the U.S. Western Interior. American Association of Petroleum Geologists Bulletin 75, 1039– 1063.

Dyer, K. R., & Huntley, D. A. (1999). The origin, classification and modelling of sand banks and ridges. Continental Shelf Research, 19(10), 1285–1330. https://doi.org/10.1016/S0278-4343(99)00028-X

FitzGerald, D.M., Buynevich, I.V., Argow, B.A. (2006). Model of Tidal Inlet and Barrier Island Dynamics in a Regime of Accelerated Sea Level Rise. Journal of Coastal Research, 789–795.

FitzGerald, D.M., Fenster, M.S., Argow, B.A., & Buynevich, I.V. (2008). Coastal Impacts Due to Sea-Level Rise. Annual Review of Earth and Planetary Sciences, 36(1), 601–647. https://doi.org/10.1146/annurev.earth.35.031306.140139

Goff, J. A., Lugrin, L., Gulick, S. P., Thirumalai, K., & Okumura, Y. (2016). Oyster reef die-offs in stratigraphic record of Corpus Christi Bay, Texas, possibly caused by drought-driven extreme salinity changes. Holocene (Sevenoaks), 26(4), 511–519. https://doi.org/10.1177/0959683615612587

Goff, J. A., Allison, M. A., Gulick, S. P. S., Reece, R., Davis, M., Duncan, D., & Saustrup, S. (2015). Shoreface ravinement evolution tracked by repeat geophysical surveys following Hurricane Ike, Bolivar Peninsula, Texas, 2008-2013. Geophysics, 80(3), WB1–WB10. https://doi.org/10.1190/geo2014-0136.1

Gould, H.R., and McFarlan, E., 1959. Geologic history of the chenier plain, southeastern Louisiana: Gulf Coast Association of Geological Societies, Transactions, v. 9, p. 261–270.

Hollis, R. J., Wallace, D. J., Miner, M. D., Gal, N. S., Dike, C., & Flocks, J. G., 2019. Late Quaternary evolution and stratigraphic framework influence on coastal systems along the north-central Gulf of Mexico, USA. Quaternary Science Reviews, 223, 105910–. https://doi.org/10.1016/j.quascirev.2019.105910

Humphrey, J. D., & Ferring, C. R., 1994. Stable Isotopic Evidence for Latest Pleistocene and Holocene Climatic Change in North-Central Texas. Quaternary Research, 41(2), 200–213. https://doi.org/10.1006/qres.1994.1022

Jarosz, E., Murray, S.P., 2005. Velocity and transport characteristics of the Louisiana–Texas Coastal Current. In: Sturges, W., Lugo-Fernandez, A. (Eds.), Circulation in the Gulf of Mexico: Observations and Models. American Geophysical Union, Washington, D. C. http://dx.doi.org/10.1029/161GM11.

Mallinson, D., Culver, S., Leorri, E., Mitra, S., Mulligan, R., & Riggs, S. (2018). Barrier Island and Estuary Co-evolution in Response to Holocene Climate and Sea-Level Change: Pamlico Sound and the Outer Banks Barrier Islands, North Carolina, USA. In Barrier Dynamics and Response to Changing Climate (pp. 91–120). Springer International Publishing. https://doi.org/10.1007/978-3-319-68086-6_3

Morton, R. A., & Donaldson, A. C. (1973). Sediment distribution and evolution of tidal deltas along a tide-dominated shoreline, Wachapreague, Virginia. Sedimentary Geology, 10(4), 285–299. https://doi.org/10.1016/0037-0738(73)90053-5

Nordfjord, S. Goff, J.A., Austin, J.A. J.R. and Sommerfield, C.K., 2005, Seismic Geomorphology of buried channel systems on the New Jersey outer shelf: Assessing past environmental conditions: Marine Geology, v. 214, p. 339–364.

Nordfjord, S., Goff, J.A., Austin Jr., J.A., Gulick, S.P.S., 2006. Seismic facies of incised valley fills, New Jersey continental shelf: implications for erosion and preservation processes acting during latest Pleistocene–Holocene transgression. Journal of Sedimentary Research 76, 1284–1303.

Nordt, L. C., Boutton, T. W., Hallmark, C. T., & Waters, M. R., 1994. Late Quaternary Vegetation and Climate Changes in Central Texas Based on the Isotopic Composition of Organic Carbon. Quaternary Research, 41(1), 109–120. https://doi.org/10.1006/qres.1994.1012

Nordt, L. C., Boutton, T. W., Jacob, J. S., & Mandel, R. D., 2002. C4 Plant Productivity and Climate-CO2 Variations in South-Central Texas during the Late Quaternary. Quaternary Research, 58(2), 182–188. https://doi.org/10.1006/qres.2002.2344

Oey, L.-Y., 1995. Eddy- and wind-forced shelf circulation. J. Geophys. Res. Oceans 100, 8621–8637.

Olsen, T.R., 1998. High-resolution sequence stratigraphy of prograding shoreface systems—a comparison between the Rannoch/Etive Formations, Tampen Spur area, northern North sea and the Point Lookout Formation, Mancos Canyon, southwest Colorado. In: Gradstein, F.M., Sandvik, K.O., Milton, N.J. (Eds.), Sequence Stratigraphy—Concepts and Application. Norwegian Petroleum Society Special Publication, vol. 8, pp. 355– 372.

Paine, J.G., 1993. Subsidence of the Texas coast: inferences from historical and late Pleistocene sea levels. Tectonophysics 222, 445–458.

Posamentier, H.W., 2002. Ancient shelf ridges—a potentially significant component of the transgressive systems tract: case study from offshore northwest Java. American Association of Petroleum Geologist Bulletin 86, 75–106.

Pirmez, C., Prather, B.E., Mallarino, G., O'Hayer, W.W., Droxler, A.W., Winker, C.D., 2012. Chronostratigraphy of the Brazos–Trinity depositional system, western Gulf of Mexico: implications for deepwater depositional models. In: Prather, B.E., Deptuck, M.E., Mohrig, D., Van Hoorn, B., Wynn, R.B. (Eds.), Application of the Principles of Seismic Geomorphology to Continental-Slope and Base-of-slope Systems: Case Studies from Seafloor and Near-seafloor Analogues. SEPM Special Publication 99, pp. 111–143.

Raff, J. L., Shawler, J. L., Ciarletta, D. J., Hein, E. A., Lorenzo-Trueba, J., & Hein, C. J. (2018). Insights into barrier-island stability derived from transgressive/regressive state changes of Parramore Island, Virginia. Marine Geology, 403, 1–19. https://doi.org/10.1016/j.margeo.2018.04.007

Reijenstein, H. M., Posamentier, H. W., & Bhattacharya, J. P., 2011. Seismic geomorphology and high-resolution seismic stratigraphy of inner-shelf fluvial, estuarine, deltaic, and marine sequences, Gulf of Thailand. AAPG Bulletin, 95(11), 1959–1990. https://doi.org/10.1306/03151110134

Riggs, S. R., Cleary, W. J., & Snyder, S. W., 1995. Influence of inherited geologic framework on barrier shoreface morphology and dynamics. Marine Geology, 126(1-4), 213–234. https://doi.org/10.1016/0025-3227(95)00079-E

Rodriguez, A., 1998. Abstract: Holocene Tidal Deltas of the Trinity Incised Valley: Analogs for Exploration and Production. AAPG Bulletin, 82 (1998). https://doi.org/10.1306/1D9BD047-172D-11D7-8645000102C1865D

Rodriguez, A.B., Anderson, J.B., Siringan, F.P., Taviani, M., 1999. Sedimentary facies and genesis of Holocene sand banks on the east Texas inner continental shelf. In: Sneddin, J., Bergman, K. (Eds.), Isolated Shallow Marine Sand Bodies. SEPM Special Publication 64, pp. 165–178.

Rodriguez, A.B., Anderson, J.B., Banfield, L.A., Taviani, M., Abdulah, K., Snow, J.N., 2000b. Identification of a −15 m Wisconsin shoreline on the Texas inner continental shelf. Palaeogeogr. Palaeoclimatol. Palaeoecol. 158, 25–43.

Rodriguez, A.B., Anderson, J.B., Siringan, F.P., Taviani, M., 2004. Holocene evolution of the east Texas coast and inner continental shelf: along-strike variability in coastal retreat rates. J. Sediment. Res. 74, 405–421.

Rodriguez, A., Anderson, J., & Simms, A. (2005). Terrace inundation as an autocyclic mechanism for parasequence formation; Galveston Estuary, Texas, U.S.A. Journal of Sedimentary Research, 75(4), 608–620. https://doi.org/10.2110/jsr.2005.050

Ronchi, L., Fontana, A., Correggiari, A., & Asioli, A. (2018). Late Quaternary incised and infilled landforms in the shelf of the northern Adriatic Sea (Italy). Marine Geology, 405, 47–67. https://doi.org/10.1016/j.margeo.2018.08.004

Ronchi, L., Fontana, A., Correggiari, A., & Remia, A. (2019). Anatomy of a transgressive tidal inlet reconstructed through high-resolution seismic profiling. Geomorphology (Amsterdam, Netherlands), 343, 65–80 https://doi.org/10.1016/j.geomorph.2019.06.026

Saustrup, Steffen & Goff, John & Gulick, Sean. (2019). Recommended "Best Practices" for Chirp Acquisition and Processing. 10.31223/osf.io/7csjh.

Simms, A.R., Anderson, J.B., DeWitt, R., Lambeck, K., Purcell, A., 2013. Quantifying rates of coastal subsidence since the last interglacial and the role of sediment loading. Glob. Planet. Chang. 111, 296–308.

Siringan, F.P., and Anderson, J.B., 1993, Seismic facies, architecture, and evolution of the Bolivar Roads tidal inlet/delta complex, east Texas Gulf Coast: Journal of Sedimentary Geology, v. 63, p. 794–808.

Siringan, F.P., Anderson, J.B., 1994. Modern shoreface and inner-shelf storm deposits off the east Texas coast, Gulf of Mexico. J. Sediment. Res. 64, 99–110.

Snedden, J.W., Dalrymple, R.W., 1999. Modern shelf sand ridges: from historical perspective to a unified hydrodynamic and evolutionary model. In: Bergman, K.M., Snedden, J.W. (Eds.), Isolated Shallow Marine Sand Bodies: Sequence Stratigraphic Analysis and Sedimentological Interpretation. SEPM Special Publication, vol. 64, pp. 13– 28.

Standring, P., Lowery, C., Burstein, J., Swartz, J., Goff, J., Gulick, S., 2019, Holocene Sea Level Rise and Paleo-environmental Change Within Trinity River Paleo-valley Offshore Galveston Bay, Gulf of Mexico: Geological Society of America Abstracts with Programs. Vol. 51, No. 5, 2019. doi: 10.1130/abs/2019AM-338683

Storms, J., Weltje, G., Terra, G., Cattaneo, A., & Trincardi, F. (2008). Coastal dynamics under conditions of rapid sea-level rise: Late Pleistocene to Early Holocene evolution of barrier–lagoon systems on the northern Adriatic shelf (Italy). Quaternary Science Reviews, 27(11), 1107–1123. https://doi.org/10.1016/j.quascirev.2008.02.009

Swartz, J.M. (2019). *Channel processes and products in subaerial and submarine environments across the Gulf of Mexico* (Unpublished doctoral dissertation). University of Texas at Austin, Austin, TX.

Swift, D.J.P., and Thorne, J.A., 1991, Sedimentation on continental margins; I, A general model for shelf sedimentation, in Swift, D.J.P., Oertel, G.F., Tillman, R.W., and Thorne, J.A., eds., Shelf Sand and Sandstone Bodies; Geometry, Facies and Sequence Stratigraphy: International Association of Sedimentologists, Special Publication 14, p. 3–31.

Thomas, M.A., 1991. The Impact of Long-term and Short-term sea Level Changes on the Evolution of the Wisconsinan–Holocene Trinity/Sabine Incised Valley System, Texas Continental Shelf. Unpublished Ph.D. Dissertation, Rice University, Houston, TX, 247 pp.

Thomas, M.A., Anderson, J.B., 1994. Sea-level controls on the facies architecture of the Trinity/Sabine incised-valley system, Texas continental shelf. In: Dalrymple, R., Boyd, R., Zaitlin, B.A. (Eds.), Incised-valley Systems SEPM Special Publication 51. Tulsa, Oklahoma, pp. 63–82.

Toomey, R. S., Blum, M. D., & Valastro, S. (1993). Late Quaternary climates and environments of the Edwards Plateau, Texas. Global and Planetary Change, 7(4), 299–320. https://doi.org/10.1016/0921-8181(93)90003-7

Vail, P.R., Mitchum Jr., R.M., Todd, R.G., Widmier, J.M., Thompson III, S., Sangree, J.B., Bubb, J.N., Hatlelid, W.G., 1977. Seismic stratigraphy and global changes of sea-level. In: Payton, C.E. (Ed.), Seismic Stratigraphy—Applications to Hydrocarbon Exploration. American Association of Petroleum Geologists Memoir, vol. 26, pp. 49–212.

Van Wagoner, J.C., Posamentier, H.W., Mitchum, R.M., Vail, P.R., Sarg, J.F., Loutit, T.S., Hardenbol, J., 1988. An overview of the fundamentals of sequence stratigraphy and key definitions. In: Wilgus, C.K., Hastings, B.S., Kendall, C.G.St.C., Posamentier, H.W., Ross, C.A., Van Wagoner, J.C. (Eds.), Sea-Level Changes—An Integrated Approach. SEPM Special Publication, vol. 42, pp. 39– 45.

Van Wagoner, J.C., Mitchum, R.M., Campion, K.M., Rahmanian, V.D., 1990. Siliciclastic sequence stratigraphy in well logs, cores, and outcrops. American Association of Petroleum Geologists Methods in Exploration Series 7 (55 pp.).

Wallace, D. J., Anderson, J. B., & Fernandez, R. A. (2010). Transgressive Ravinement versus Depth of Closure: A Geological Perspective from the Upper Texas Coast. Journal of Coastal Research, 26(6), 1057–1067. https://doi.org/10.2112/JCOASTRES-D-10-00034.1

Zaitlin, B.A., Dalrymple, R.W., Boyd, R., 1994. The stratigraphic organization of incised-valley systems associated with relative sea-level change. In: Dalrymple, R.W., Zaitlin, B.A., Scholle, P.A. (Eds.), Incised-Valley Systems: Origin and Sedimentary Sequences. SEPM Special Publication, vol. 51, pp. 45– 60.

Zecchin, M., Brancolini, G., Tosi, L., Rizzetto, F., Caffau, M., & Baradello, L. (2009). Anatomy of the Holocene succession of the southern Venice lagoon revealed by very high-resolution seismic data. Continental Shelf Research, 29(10), 1343–1359. https://doi.org/10.1016/j.csr.2009.03.00